Student thesis series INES nr 675

Early detection of bark beetle attacks:

Integrating Segment Anything Model (SAM) zero-shot segmentation and spectral indices for tree health assessment

Marianne Olsson

2024
Department of
Physical Geography and Ecosystem Science
Lund University
Sölvegatan 12
S-223 62 Lund
Sweden

Marianne Olsson (2024).
Early detection of bark beetle attacks: Integrating Segment Anything Model (SAM) zero-shot segmentation and spectral indices for tree health assessment
Master degree thesis, 30 credits in *GIS and Remote Sensing*
Department of Physical Geography and Ecosystem Science, Lund University

Level: Master of Science (MSc)

Course duration: *January* 2024 until *June* 2024

Early detection of bark beetle attacks:

Integrating Segment Anything Model (SAM) zero-shot segmentation and spectral indices for tree health assessment

---

Marianne Olsson

Master thesis, 30 credits, in *Master of Science (MSc)*

Per-Ola Olsson
Lund University

Shangharsha Thapa
Lund University

Exam committee:
José Beltrán, Lund University
Anna Maria Jönsson, Lund University

Abstract

Forests offer vital ecosystem services but face threats from various stressors, including climate change and insect infestations. The European spruce bark beetle (*Ips typographus L.)* poses significant risks to Norway Spruce (*Picea abies*). Early detection of bark beetle infestations is crucial for damage control but challenging with traditional methods. This study aims to utilize modern remote sensing technologies, particularly high-resolution Unmanned Aerial Vehicle (UAV) imagery, combined with the Segment Anything Model (SAM) to segment individual spruce trees and detect early signs of bark beetle attacks. Field studies were conducted in Mulatorp, a nature reserve in southeast Sweden, capturing UAV images over several months. The SAM, a state-of-the-art deep learning model for image segmentation, was used to segment individual spruce trees from RGB UAV data. The study aimed to assess SAM's zero-shot capabilities, refine its segmentation parameters, and compare its outputs with manually validated data. Additionally, the study sought to develop a time-series of vegetation indices to detect early signs of bark beetle infestations.

Results indicated that SAM's box prompts yielded better segmentation accuracy than point prompts, though the model often merged canopies and missed some trees. Despite the high spatial resolution of UAV imagery, SAM detected only 37% of all trees and 33% of Norway spruce trees, with an IoU of 0.55 for spruce trees. The Green Chromatic Coordinate (GCC) was identified as the most effective vegetation index for early detection, showing significant differences between healthy and attacked trees as early as June. The findings suggest that while SAM has potential for remote sensing applications, its current zero-shot capabilities are insufficient for precise tree segmentation without further refinement and training. The study highlights the importance of integrating advanced segmentation models with UAV imagery for effective forest health monitoring and early intervention in bark beetle infestations. Future research should focus on enhancing SAM’s segmentation accuracy and expanding field-validated datasets to improve early detection frameworks.

Acknowledgements

I want to thank Per-Ola Olsson and Shangharsha Thapa from Lund University for their support and guidance for this master thesis. The data used for the study was also provided by them. Furthermore I also want to thank José Beltrán and Anna Maria Jönsson from Lund University for the support and feedback.

1 Introduction 1
1.1. Aims and objectives 3
2 Background 4
2.1. Bark beetle ecology, impacts, and climate change 4
2.2. Remote sensing and spectral vegetation indices (SVIs) 6
2.3. Object detection and segmentation 7
2.4. Monitoring and detection of bark beetle attacks 9
2.4.1 Bark beetle detection 9
2.4.2 Spruce bark beetle 10
3 **Study area and data** 11
3.1 Study area 11
3.2 Data 12
3.2.1 UAV imagery capture and processing 12
3.2.2 Field data 14
4 **Methods** 14
4.1. Empirical line correction of orthomosaics 15
4.2 Tree segmentation 17
4.2.1 Model architecture 18
4.2.2 Model parameters 19
4.2.3. Zero shot segmentation and post-processing 20
4.2.4 Validation data creation 20
4.2.5 SAM validation metrics 21
4.3 Vegetation Indices calculation and time series 23
5 **Results** 24
5.1 SAM segmentation results 28
5.2 Time series of individual bands and vegetation indices 32
6 **Discussion** 36
6.1 Capability of SAM for individual tree crown delineation 36
6.1.1 Zero-Shot performance and prompted segmentation 37
6.1.2 Comparison with validation data and limitations 37
6.1.3. Future prospects of SAM for tree crown delineation and remote sensing applications 39
6.2 Spectral response and detection of attacks 40
6.2.1. Problems with the data, limitations 42
6.1.3 Future studies: bark beetle health monitoring and individual tree crown delineation 42
7. **Conclusion** 43
References **44**

List of abbreviations

UAV – Unmaanned Aerial Vehicle

NIR – Near infrared

R – Red band

GCC – Green Chromatic Coordinate

RCC – Red Chromatic Coordinate

NDVI – Normalized Difference Vegetation Index

NDRE - Normalized Difference Red-Edge Index

SAM – Segment Anything Model

IoU – Intersection Over Union

DN – Digital Number

CNN – Convolutional Neural Network

CHM – Canopy Height Model

1 Introduction

Forests provide numerous ecosystem services, such as timber and pulpwood, bioenergy, climate regulation, and recreation (Hansen & Malmaeus, 2016). However, there are various abiotic and biotic stressors that threaten our forests. One example of such is climate change, which intensifies droughts and weather extremes (Jactel et al., 2012; Marini et al. 2013). Coupled with this is insect damage. Insect damage causes severe ecological and economic damage (Huo et al., 2023). The European spruce bark beetle (*Ips typographus* L.) is an example of such, being an aggressive species that is a threat to Norway Spruce (*Picea abies* (L.) Karst).

Bark beetles are naturally present in spruce forests at lower populations. However, there are certain conditions that allow for their rapid population growth, allowing them to attack healthy trees. Such conditions are warmer climates, drought events, and windstorms (Jactel et al. 2012; Netherer et al. 2019; Schelhaas et al. 2003). As an example, the largest documented outbreak in Sweden was triggered by the 2018 drought killing more than 31 million m^3 of spruce trees during the period 2018-2022 (Schroeder 2023). Such a destruction causes not only economic losses but also poses a serious threat to forest ecosystems (Huang et al., 2019). It is therefore important to use and develop methods to monitor these outbreaks to prevent the further spread of bark beetles, especially in the early infestation stages.

Early detection of bark beetle infestations can be challenging due to several reasons. The only visible symptoms of the initial colonization phase are entrance holes of beetles in the tree trunks, brown sawdust and fresh resin flow which are costly and difficult to detect in the field (Honkavaara et al. 2020). The colour of the tree crown gradually changes from green to yellow, and finally to reddish brown and grey in the final stage when the tree dies. At the early infestation stage, the crowns of the attacked trees often stay green, coining the term “green attack” in remote sensing (Wulder et al. 2006). In this phase, the larvae are still under the bark. Identifying attacked trees at an early stage is vital for damage control if they can be removed from the forest to control the population and reduce the potential damage caused by the future bark beetle generations (Huo et al. 2023).

Remote sensing has shown promising methods for bark beetle attack detection, providing a more effective approach that field surveys. Numerous studies have demonstrated the capabilities of satellite imagery for bark beetle detection (Fernandez-Carrillo et al. 2020, Migas-Mazur et al. 2021, Safonova et al. 2019). However, challenges remain when detecting bark beetle attacks, such as cloud-covers which result in gaps in the time-series, and low spatial resolution that hinders individual level detection (Zabihi et al. 2021; Kautz et al. 2024).

Modern remote sensing technologies, such as high-resolution Unmanned Aerial Vehicle (UAV) imagery, provide high spatial resolution images that can be used to monitor forest health particularly for detecting spruce bark beetle attacks (Barta et al., 20; Honkavaara et al., 2020; Huo et al 2023). In contrast to other remote sensing techniques such as satellite imagery, UAV data allows for a flexible way to acquire data since the type of sensor, angles of view, time, and frequency of acquisition can be controlled by the user (Alvarez et al. 2021). Moreover, UAV data acquisition in comparison to manned aerial vehicles is more cost effective, more user friendly, and faster.

Images based methods to detect bark beetle infestations are usually based on the crown discoloration caused by disrupted water and nutrient transport of the attacked trees (Turkulainen et al. 2023). Such image-based methods include vegetation indices derived from multispectral images. Generally, water-stressed trees reflect a higher amount of visible light than healthy trees (Ortiz et al., 2013). Research indicates stress from lack of water impacts a tree's chlorophyll levels, which leads to decreased visible light absorption (Blackburn, 1998, 2006; Carter & Knapp, 2001). This stress is also linked to a rise in the reflection of Red-Edge light as a result of both diminished chlorophyll *a* levels and changes in the spongy mesophyll's structure. Furthermore, these alterations in the spongy mesophyll are associated with reduced near-infrared wavelength absorption in water-stressed trees (Ortiz et al. 2013; Trubin et al. 2023).
To detect attacked trees, it is important to delineate their areas images, identifying pixels belonging to each tree. Deep learning methods provide a useful tool for individual crown segmentation. Image analysis tasks and object detection, a commonly used deep learning method are convolutional neural network (CNN) (Zhao

et al., 2023). CNN models have achieved high accuracies in both individual tree detection and crown delineation (Xiao et al. 2020; Lou et al. 2022; Chadwick et al. 2020; Wu et al. 2020), but require vast amounts of training data and computational capacity.

Segment Anything Model (SAM) was released by Meta in April 2023, a state-of-the-art model for image segmentation. The main advantage of this model is that it can segment images without prior specific training and works efficiently with high resolution datatsets for segmenting objects of interest. SAM was trained with 11 million images, creating 100 masks per image, thus having 1 billion masks in total (Hu et al., 2023). SAM has promptable features and also has zero-shot capabilities (machine learning technique that allows a model to classify objects from unseen classes).

To my knowledge, there are very few papers assessing the zero-shot capabilities of SAM in a remote sensing context, especially in forest settings. There are papers on precision agriculture, and within the field of medical imaging (Carraro et al. 2023; Gui et al. 2024; Hu et al. 2023). Since it is a fairly new algorithm that was released in 2023, this paper aims to fill the gap of applying SAM to the context of precision forestry and assessing SAM's zero-shot capabilities to produce individual tree segments.

1.1. Aims and objectives

Bark beetle infestations have devastating effects to the forest ecosystem and the economy. Finding ways to utilize modern AI methods and high-resolution imagery can be crucial to monitor spruce bark beetle attacks. The main aim of this thesis is to segment individual spruce trees using Segment Anything Model (SAM) with RGB UAV data automatically. SAM has shown promising capabilities in other applications, and investigating its capacity in a forested area has not yet been investigated. These segments will then be used to create a time-series of different vegetation indices for the segments, thereby enabling bark beetle attacked trees monitoring.

- How accurately can SAM delineate individual tree crowns in a zero-shot setting with RGB images?

- Is the output of SAM sufficient for the segmentation and vegetation calculations for UAV images?
- How early can we detect bark beetle attacks using indices from high resolution RGB images?
- How early can we detect bark beetle attacks using indices from high resolution multispectral UAV data?

The hypothesis of this thesis are outlined below.

Hypothesis 1: SAM will demonstrate a satisfactory accuracy for automatically segmenting individual spruce trees in a zero-shot setting using RGB data.

Hypothesis 2: The time-series of RGB indices, Red-Edge, and NIR bands and spectral indices will enable the early differentiation of bark beetle attacks in forest, which can aid in mitigating their impacts on forest ecosystems.

2 Background

This section covers facts about the bark beetle, machine learning for image segmentation, and methods for bark beetle detection to provide context to the study.

2.1. Bark beetle ecology, impacts, and climate change

Forest insects are a vital part of the forest ecosystem as they consume dead wood and renew weakened forests, aiding the nutrient and carbon cycling in these ecosystems. Bark beetles, belonging to the family Coleoptera and subfamily Scolytinae, encompass around 6000 species worldwide. These insects, named for their reproductive habits within the inner bark of trees, primarily feed on the phloem, or true bark beetles, of woody plants. However, only a fraction of these species, as highlighted by Bentz and Jönssön (2015), Raffa et al. (2008), and Öhrn (2012), are known to cause significant economic damage by killing healthy trees.

A notable species causing concern is the spruce bark beetle (Ips typographus L.), prevalent in Europe and Asia. This beetle poses a significant threat to the Norway spruce (Picea abes (L.) Karst), and like other bark beetles, is ectothermic, relying on external temperature for metabolism and development (Öhrn 2012). The adult beetles typically overwinter under the bark or in soil and forest litter. With the onset of warmer spring temperatures exceeding 18ºC, they begin their flight, seeking breeding

material across forests (Öhrn 2012). Their breeding behaviour varies; they utilize wind-felled trees during non-outbreak periods and attack healthy trees during outbreaks, as described by CABI (2022). The initiation of attacks involves males constructing nuptial chambers in the bark and emitting pheromones to attract females, who then lay 50-80 eggs in constructed galleries within the bark (Kimoto and Duthie-Holt, 2006).

Norway spruce trees, like many conifers, have natural defense mechanisms against such insect infestations, comprising both a physical barrier (bark) and toxic chemicals in the phloem and xylem. These defences, triggered by wounds, are typically effective against bark beetles. However, during periods of stress, like drought, or during outbreaks, these mechanisms can be overwhelmed, leading to significant tree loss as the beetles disrupt nutrient and water transportation (Öhrn 2012).

The frequency of spruce bark beetle generations is climate dependent. While traditionally univoltine in Northern Europe, producing one offspring generation per year, there has been a noted shift towards bivoltism, with two generations per year becoming more common as observed in studies like Lange et al. (2006) and Öhrn (2012). The latter noted that flight commencement now occurs over two weeks earlier than three decades ago in Southern Sweden, with a second generation often initiated but not completed.

Climate change exacerbates the risk of bark beetle outbreaks through both direct and indirect effects. Directly, increased temperatures can lead to earlier maturation and swarming, potentially resulting in an additional generation annually (Ökland et al. 2015). A modelling study by Jönsson et al. (2012) also predict an increased frequency of attacks and the likelihood of one more generation to completing annually due to warming climates in Sweden. Indirect effects, such as drought and wind-felling, also significantly contribute to outbreaks and are expected to increase with climate change (Jactel et al., 2019; Seidl et al. 2017). Historically, European spruce bark beetle outbreaks were primarily storm-induced, but recent years have seen a rise in drought-induced outbreaks, with the 2018 drought triggering the largest recorded outbreak (Hlásny et al. 2021).

2.2. Remote sensing and spectral vegetation indices (SVIs)

Remote sensing is the science and practice of obtaining information about objects or areas from a distance using electromagnetic radiation. This field of studies has evolved over time, employing various methods and sensors which are tailored to specific research and a widespread application in environmental monitoring. The launch of the first Earth observation satellite in the early 1970s marked a milestone, allowing public access to data about the Earth's surface at relatively low costs. This development opened the door to multitemporal data collection, enabling the observation and analysis of environmental changes over time. The 1990s saw further advancements, notably in spectral resolution, enhancing the capability for detailed environmental monitoring. Particularly, satellite based remote sensing techniques have aided in vegetation health monitoring. However, a resolution of less than 4 m is needed to be able to detect individual attacks, particularly in early detection of bark beetles more accurately (Zabihi et al. 2021). Another prevailing issue in using satellite-based methods is that cloud covers present in the images can cause gaps in the time-series creations, especially in the Nordic regions (Krautz et al. 2024).

An alternative to satellite-based methods is using UAVs. UAVs have shown the potential to bridge the gap between field observations and satellite imagery, since low altitude flights produce high resolution images (0.02-0.04 m) and is less affected by clouds. Moreover, UAV data allows for a flexible way to acquire data since the type of sensor, angles of view, time, and frequency of acquisition can be controlled by the user (Alvarez et al. 2021).

Another aspect in remote sensing is the development of sensor technology. Advancements in sensor technology such as Red, Green, Blue (RGB) cameras, multispectral, hyperspectral, and thermal sensors have aided in vegetation mapping. Vegetation's response across the electromagnetic spectrum, captured by these sensors, is indicative of its health. For example, RGB cameras record visible light (400-700 nm), useful in detecting changes in foliage pigmentation and greenness associated with stressors like bark beetle attacks. Specifically, stressed trees because of beetle activity, exhibit increased reflectance in the visible and Red-Edge bands, linked to chlorophyll loss and changes in mesophyll structure (Zabihi et al. 2021b; Ortiz et al. 2013). These changes are crucially captured by near infrared (NIR) and Red-Edge

bands, part of multispectral sensors. The Red-Edge region (680-750 nm) is especially informative, highlighting the shift from chlorophyll absorption to cellular scattering.

By integrating high resolution UAV images, RGB, NIR, and Red-Edge data, multispectral UAV data facilitates the computation of vital vegetation indices. These indices, reflecting different aspects of plant health, are instrumental in diagnosing and analysing forest health, particularly in the context of bark beetle infestation impacts. Several spectral vegetation indices are used for vegetation health monitoring, the most common one being the normalized difference vegetation index (NDVI). NDVI relies on the fact that healthy vegetation reflects a lot of light in the NIR spectrum, contrasting with non-vegetation objects. It combines Red (R) and NIR bands as a ratio. Red-Edge NDVI is also an index used for estimating vegetation health using the Red-Edge band and is especially useful for estimating vegetation health in the mid to late stages of growth, when the chlorophyll concentration is relatively higher (Ortiz et al. 2013). Chromatic indices such as Green Chromatic Index (GCC) and Red Chromatic Index (RCC) are simple measures of the phenological traits of vegetation. GCC provides a measure of the greenness of the canopy. Both RCC and GCC are indices that has been used in numerous studies as a robust metric to characterize the canopies' seasonal changes and for tree health monitoring (Richardson et al. 2018).

2.3. Object detection and segmentation

Image segmentation involves dividing images into meaningful and non-overlapping regions. One major aspect of computer vision involves dividing images into regions of interest by grouping pixels according to their color and texture. Image segmentation has various applications, such as in autonomous driving, medical imaging, and remote sensing. For example, tree segmentation is a desirable product for forest inventories and precision forestry (Miraki et al. 2021).

Traditional image segmentation techniques in remote sensing often rely on pixel-based or object-based approaches. Pixel-based methods, such as clustering and thresholding, involve grouping pixels with similar characteristics, while object-based techniques focus on segmenting images based on properties of larger regions or objects (Hossain and Chen, 2019). However, these methods can be limited in their

ability to handle the complexity, variability, and high spatial resolution of modern remote sensing imagery (Kotaridis and Lazaridou, 2021). Object detection aims to identify and locate objects within images or 3D data, often resulting in bounding boxes. Instance segmentation goes a step further by delineating the exact boundaries of individually detected objects. Traditional methods for image segmentation include region growing, k-means clustering, and watershed algorithms. Watershed approaches, for instance, are commonly used to delineate individual tree crowns, achieving relatively good accuracies (Qui et al, 2020; Jing et al. 2014; Huo et al. 2023).

Over the last decade, deep learning methods have been developed, such as U-Net, SegNet, Mask R-CNN, and DeepLab (Guo et al. 2023; Lv et al. 2023). Convolutional Neural Networks (CNNs) have become a popular choice in remote sensing applications due to their ability to capture local and hierarchical patterns in images. However, most segmentation algorithms rely on a large amount of data for training models, which can be time-consuming, costly, difficult to obtain, and computationally demanding (Li et al. 2023).

Meta AI's Segment Anything Model (SAM) represents a new category of 'foundational models', similar in concept to ChatGPT. These models are trained on extensive and diverse datasets, enabling their potential application across various research fields. SAM is promising due to its promptable segmentation and zero-shot capabilities, which is a model's ability to accurately process new, unseen input data. SAM’s promptable features also allow for segmentation with minimal input, using a bounding box, single point, or text as guidance (Kirillov et al., 2023). Zero-shot segmentation is a method used for image segmentation that employs unlabeled data. Various studies have explored SAM’s zero-shot capabilities with natural images, such as in rock images, crops, terrain mapping, and leaf segmentation (Ma et al. 2023; Li et al. 2024; Williams et al. 2023). A recent study of SAM in remote sensing indicates that it has potential for remote sensing applications. Currently, there are no studies focusing on delineating trees in a forest using high-resolution UAV imagery, zero-shot, and SAM. As bark beetle attacks occur at the tree level, an important goal for current and future studies is to work with individual tree scales.

Several studies on individual tree crown delineation algorithms exist, and it is a developing field of study in remote sensing. It is crucial to have algorithms that allow for automated and accurate approaches to aid in precision forestry and bark beetle detection.

2.4. Monitoring and detection of bark beetle attacks

2.4.1 Bark beetle detection

Bark beetle infestations, though relatively straightforward to identify on the ground, present unique challenges for early detection. Terrestrial signs such as red-brown frass in bark crevices and small pitch tubes protruding from the bark are classic symptoms (Kimoto and Dutchie-Holt, 2006). Additionally, infested conifers may show woodpecker damage and a progression of needle discoloration, from yellow-green to reddish-brown, before eventually shedding their needles. Methods to study the behaviour and monitor bark beetle populations like pheromone-baited traps and walking stand transects by foresters, have been effective but are often labour-intensive, time-consuming, and costly (Lausch et al. 2013).

A key challenge in early detection is the timing of visible symptoms. While terrestrial signs can be observed early in the infestation process, remote sensing typically identifies changes in the later stages, marked by a decrease in chlorophyll or water content in the canopy (Krautz et al., 2024). In remote sensing applications, infested trees are usually categorized into three stages based on crown discoloration: green-attack, red-attack, and grey-attack (Wulder et al. 2006).

The history of remote sensing for bark beetle detection extends back to the late 1920s, with the use of small aircrafts in North America for this purpose (Yuill and Eaton 1994). This century-long research journey has seen significant advancements in aerial imagery, leading to improved detection accuracies, especially for late-stage infestations such as those observed in Ponderosa pine in the late 1950s (Heller et al. 1959). In Sweden, a study on detecting spruce bark beetle in Norway spruce trees was conducted by Arneberg et al. (1973), revealing a linear correlation between the time after attack and the rate of detection. The advent of Earth monitoring satellites like Sentinel and Landsat, followed by the introduction of UAV imagery, has enhanced the spectral, temporal, and spatial resolutions, fostering optimism for better and earlier detection rates.

2.4.2 Spruce bark beetle

The potential of utilizing Unmanned Aerial Vehicles (UAVs) for early detection of spruce bark beetle infestations has been demonstrated through various studies over the years. Kloucek et al. (2019) effectively used a low-cost UAV-mounted sensor to classify different stages of bark beetle infestation. They detected treetops with canopy height models (CHM) and local maxima filtering, along with manually correcting.
Barta et al. (2022) found that remote sensing methods could detect infested trees as early as six weeks post-infestation, a crucial window for taking preventative measures against further spread, albeit using manual methods to select polygons of Norway spruce forests in different stages of bark beetle infestation. Huo et al. (2023) extended this understanding by using multispectral drone images before and during infestation periods, revealing that infestations were detectable between 5-10 weeks, with earlier detection rates at 15% and increasing to 90% at the 10-week mark. They perform individual tree segmentation using the green band with local maxima to detect treetops to be used for marker-controlled watershed segmentation.

Further contributions by Turkulainen et al. (2023), Safonova et al. (2019), and Schaeffer et al. (2021) emphasize the efficiency of combining UAVs with deep learning and machine learning techniques for early detection. Turkulainen et al. (2023) study highlights the performance of multispectral and hyperspectral imaging over RGB when processed with deep neural networks. Safonova et al. (2019) implemented a two-stage CNN architecture to successfully identify fir tree damage from bark beetles in UAV RGB images. Schaeffer et al. (2021) complemented these findings by using thresholding cellular automata in drone imagery to accurately classify infestation stages. Näsi et al. (2018) further illustrated the accuracy of UAV-based hyperspectral imaging in urban forest settings, pinpointing infested trees at an individual level.

Collectively, these studies show that integrating UAV technology with advanced image analysis can make early detection of bark beetle attacks feasible and increasingly precise. This synergy of remote sensing technologies and analytical algorithms is crucial in the fight against bark beetle infestations, offering a promising tool for forest health management and conservation efforts.

3 Study area and data

This section outlines the data collection, study area location, and pre-processing steps performed with the data before using it.

3.1 Study area

The drone flights were conducted in Mulatorp, a nature reserve in southeast Sweden (56.4194° N, 14.4854° E), approximately 60 ha in size. This part of Mulatorp was a traditionally managed forest until the 1980s, featuring various tree densities and types. Due to its ecological and historical importance, it has become a nature reserve (Länssyrelsen Blekinge, n.d). This area had an ongoing bark beetle outbreak, making it crucial to monitor the attacked trees to mitigate further damage (Figure 1). The study area consists of a mixed coniferous forest with a few deciduous trees. The study was divided into three separate areas, refer to section 4 for more details.

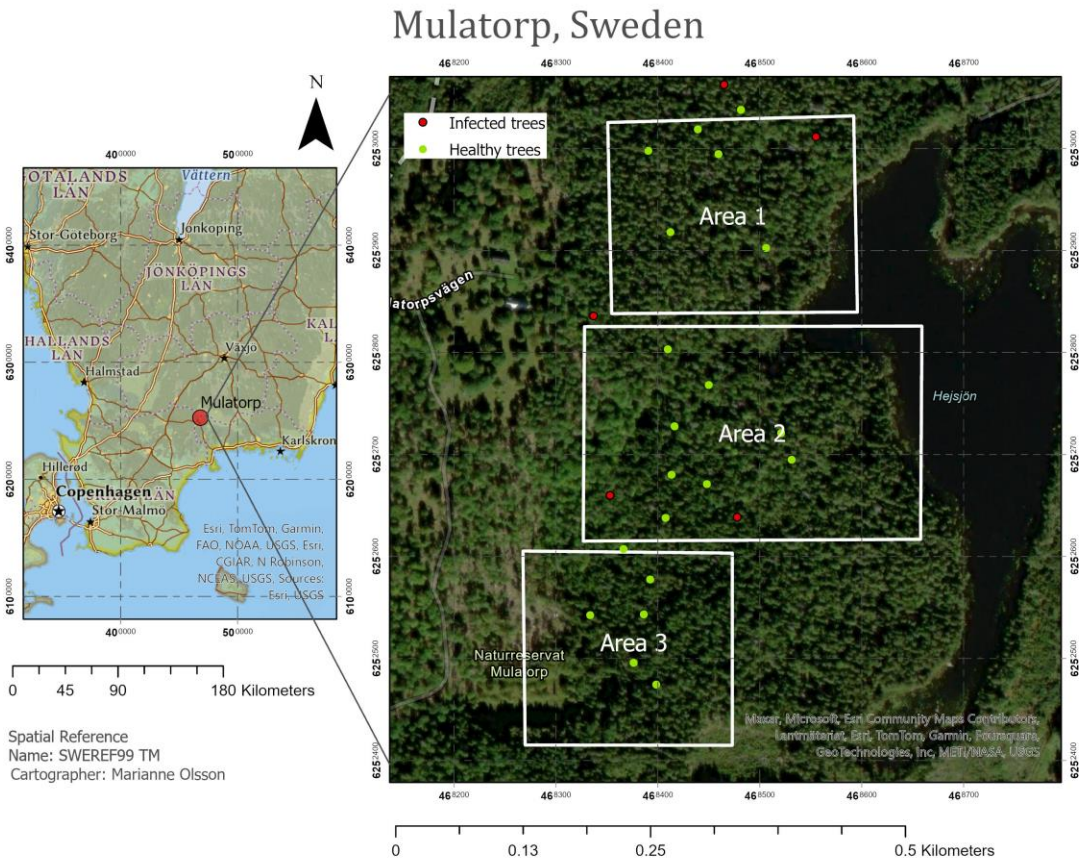

Figure 1. Study area map with an image from November 2022 showing the infected trees in red dots and healthy trees in green dots.

3.2 Data

3.2.1 UAV imagery capture and processing

A total of 12 flights were done with around 2-week intervals during May 17-November 18, 2022 (Table 2). RGB and multispectral drone images were captured using the DJI Phantom 4 Multispectral drone, a high precision drone with six cameras and ½.9 inch CMOS sensors and RTK. The 5 cameras cover the bands Blue (B), Green (G), Red (R), Red-Edge (RE), and Near-infrared (NIR) (Table 1). The resolution is 5 cm for all the bands.

Table 1. The bands of DJI Phantom 4 multispectral drone and their corresponding wavelenghts.

Bands	**Wavelength (nanometers)**
Blue (B)	450 ± 16 nm
Green (G)	560 ± 16 nm
Red (R)	650 ± 16 nm
Red-Edge (RE)	730 ± 16 nm
Near-infrared (NIR)	840 ± 26 nm

The camera and images settings were identical for all flights. During the flight the incoming radiation was recorded by the sunshine sensor on the UAV. To normalize the images for variations in incoming sunlight and facilitate reflectance calculations, data from the UAV flights' sunshine sensor were extracted from the image metadata. This involved plotting the incoming light conditions for each band (R, G, B, RE, and NIR). The UAV flights that contained irregular and complex light variability during the flights were removed. The data with constant light, under either sunny or overcast sky were kept for further processing.

The flights were categorized into three categories: (1) consistent sunny incoming light, (2) consistent cloudy incoming light with slight variation, and (3) complex incoming light. After the categorization of the flights, each image from the flights were subjected to exposure calibration, vignetting correction, and radiance

normalization. These corrections were performed based on a recently developed methodology by Olsson et al (2021). Vignetting is the phenomenon in which the image brightness is reduced from the optical centre of the image towards its edges (Bal and Palus 2023). The method to minimize the vignetting effect was based on the use of vignetting polynomial derived from the metadata of the images. More details on the exposure, vignetting, and irradiance normalization were based on and explained in Olsson et al. (2021). The corrected images were then processed in Metashape software to create georeferenced orthomosaics, based on the method used by Thapa et al. (2021). The precise geolocation of the orthomosaic is from a Swedish positioning service called SWEPOS with an accuracy of ~ 2 cm. All flights were kept at 90 m flying height, with 2m/s speed and with an 80% side and front overlap. The processing of the orthomosaic were done by the department. As a result, 3 separate orthomosaics were created, and clipped for the study where the area coverages are shown in Figure 1. The orthomosaics were clipped to remove the blurry edges where the image overlap is low, and these areas will be worked with in parallel as they cover different parts of the Mulatorp study area.

Table 2. The flight dates and the corresponding weather conditions during the flights

Flight date	Weather
22-05-17	Sunny conditions
22-06-06	Mostly homogenous cloudy conditions
22-06-22	Mostly homogenous cloudy conditions with some sunny spots for the early flights.
22-07-03	Area 1: Mostly stable cloud conditions – a few sunny spots. Area 3 : Cloudy with a few sunny spots.
22-07-23	Stable cloudy conditions with shorter periods with drizzle.
22-08-08	Mostly stable cloudy conditions.
22-08-23	Cloudy mostly stable light conditions.
22-09-08	Cloudy mostly stable light conditions.

22-09-24	Stable conditions for all seven flights.
22-10-18	Mostly stable cloudy conditions with a few brighter spots.
22-11-05	Area 1 and Area 2 in rather stable cloudy conditions. No flights at Area 3.
22-11-18	Area 1: First flight cloudy until last part. Area 2: Flight mostly sunny Area 3: Cloudy condition, but occasionally light snowfall.

3.2.2 Field data

The mutli-temporal images were used to find Norway spruce trees that were potentially attacked by bark beetles. Infected trees were identified through the orthomosaics UAV images, comparing the images of the dates in June, August, October, and November to see the development of the trees, and note the possibly infected ones, which resulted in a number of 35 trees. This was verified in the field a year later in February 2023 to inspect and confirm the bark beetle infested trees. The method of identification was to check for damage of the bark. Additionally, the trees were noted whether they were attacked early or late in the summer. 12 trees were confirmed to be infected in the field. Due to the low accuracy of GPS in the forest, not all trees were confirmed. This field work was performed by the department. From these 12 trees, 4 trees were found in the orthomosaics to be suitable for use for vegetation index calculations. Figure 2 shows the field photos taken on February 2023 for some of the confirmed trees. All 4 trees had visible sign of bark damage in the higher up in the bark and has visible strong red colouring.

4 Methods

The workflow is illustrated as follows (Figure 2) where orthomosiac creation and radiometric calibration was performed on the UAV data. From these images, healthy

and attacked trees were digitized from the field data and manual search. The UAV data was then used to calculate vegetation indices. To perform the segmentation, a small subset of the Area 1 was used to fine tune the parameters of the SAM model. This was done by changing the parameters and checking which yielded the best delineation between the trees. After the best parameters were chosen, the areas were split into tiles and ran for segmentation. A random subset of the tiles were chosen as validation data, about 20% of the tiles were used as validation and digitized using semi-automatic segmentation with box prompts and point prompts, a feature of SAM integrated with QGIS created by Zhao et al. (2023). Finally, the time series were created using the healthy and attacked trees data created in the second step. It is important to note that for the vegetation indices calculations, manually digitized trees were used instead of the SAM output. This is because the segments were not accurate enough for the intended index calculations.

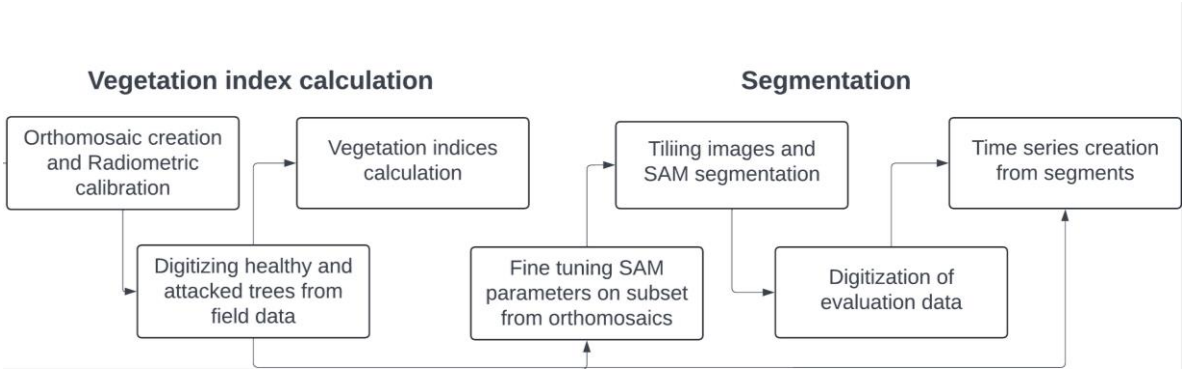

Figure 2. An outline of the workflow performed.

4.1. Empirical line correction of orthomosaics

Finally, radiometric calibration is needed to convert DN into reflectance values. Surface reflectance is not directly measured by the UAV cameras as light/radiant energy is recorded by the image sensor per pixel as a digital number (DN). A commonly used method to convert DNs to surface reflectance is the empirical line method (Smith and Mitlon, 1999). This method assumes a linear relationship between surface reflectance and (R) and radiance recorded by the sensor (L) (Figure 3.). To perform this, at least two reflectance panels are needed with their standard reflectance values (Table 1.).

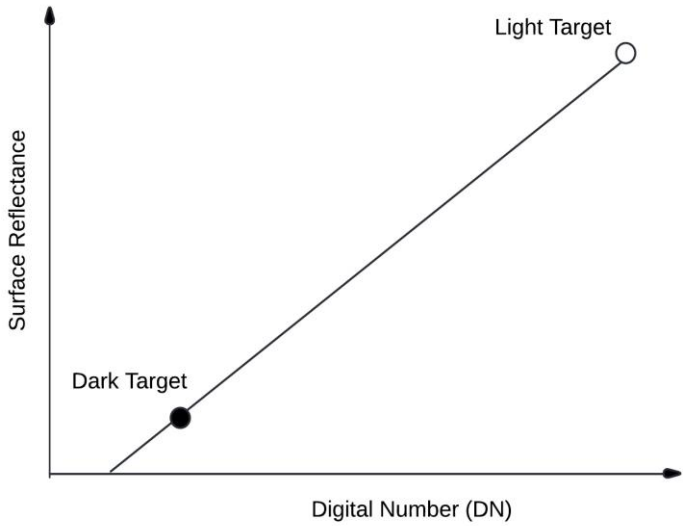

Figure 3. Empirical line method from Smith and Milton (1999).

The empirical line equation was derived from reflectance calibration panels in the corrected individual images (Figure 5). The software used was a produced script which took the mean DN values per panel per image (SITES, 2023). The RGB bands are notably saturated and therefore was not radiometrically calibrated. Instead, raw bands were used. Standard reflectance values were provided by the manufacturer, Altisense company (Table 3).

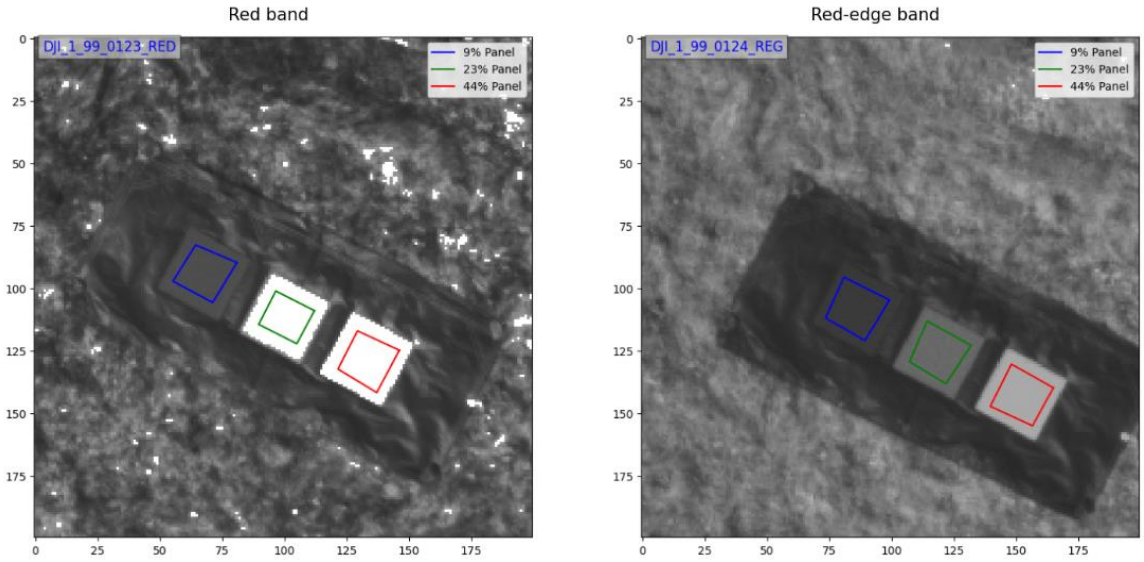

Figure 4. Reflectance panels for radiometric calibration and the method used to extract DN values. The red band panels are notably saturated, making it challenging to calibrate with the empirical line method.

Table 3. Reflectance calibration panels and their resulting values for each band.

Band	**9%**	**23%**	**44%**
Blue	0.071864034	0.217418623	0.382620256
Green	0.068064604	0.218853955	0.45281708
Red	0.076557511	0.22275384	0.43940517
Red-Edge	0.084988391	0.234725921	0.466921599
NIR	0.100331593	0.251634465	0.497430071

The standard reflectance of the panels and the mean DN of the panel were used to convert the orthomosaics into reflectance using the empirical line equation as seen in Equation (1).

$$R = a \times DN_{corr} - b$$

.....(1)

Where R is the reflectance, DN_{corr} is the radiometrically corrected DN value after the pre-processing steps, a is the slope of the regressioon line, and b is the intercept. After these steps, the calibrated NIR and Red-Edge bands and the raw RGB bands will be used to calculate vegetation indices to assess healthy and attacked trees. The resulting digitized trees from the aforementioned steps will be used to get the mean values for the vegetation indices and time series creation.

4.2 Tree segmentation

This part covers the architecture of the model used for tree segmentation, and accuracy metrics used to analyse the model performance. SAM is currently freely accessible, and the source code is made open access. Using SAM for image segmentation is straightforward. It compromises of two main functions, the interactive and manual selection of target points, text or bounding boxes as input prompts, and the automatic mask generator where SAM autonomosly does the image segmentation process, given that the parameters are fine tuned to the data.

4.2.1 Model architecture

SAM comprises three key components: a promptable segmentation task, a segmentation model (SAM) that enables zero-shot capabilities from input prompts, and a data engine (SA-1B) that collects a dataset of over 1 billion prompts. The basic architecture of image segmentation includes an encoder and a decoder (Figure 5). The encoder extracts features from the image using filters, utilizing deep convolutional neural networks (CNN). The mask encoder employs a ViT-H/16 transformer model, which handles 16x16 patch sizes. The encoder extracts rich semantic information from the input image through convolutional and pooling operations, increasing the number of channels while decreasing geographical dimensions to gather both local and global contextual data. The SAM model uses CNNs to extract hierarchical properties from input images, with deeper layers capturing more abstract representations. The decoder reconstructs the segmentation mask from the encoder's low-resolution feature maps through operations like transposed convolutions or nearest-neighbor interpolation. It also includes skip connections linking appropriate encoder and decoder layers. The decoder generates the final output, typically a mask outlining the objects (Guo et al., 2023).

The spatial analysis was conducted using a custom tool, "SamGeo," part of the original SAM module. SAM has different models available, including ViT-H, ViT-L, and ViT-B, each with varying computational requirements and architecture (Kirillow et al., 2023). This study used the ViT-H SAM model, the most advanced and complex model available. The automatic mask generator created masks from the images, with adjustable parameters to produce task-specific masks.

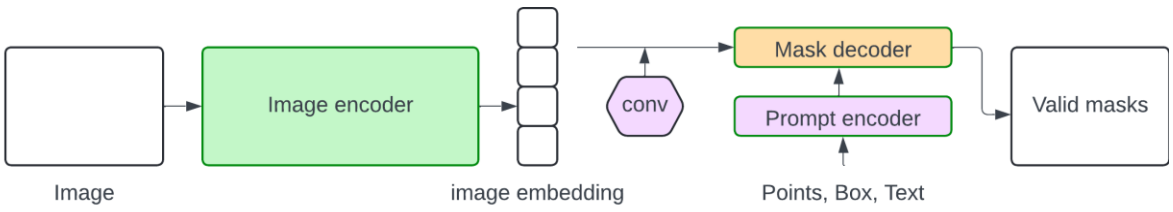

Figure 5. The model architecture adapted from Kirillov et al (2023) showing the Segment Anything Model (SAM)'s overview. An image encoder outputs an image embedding that can be efficiently queried by various input prompts to produce object masks.

4.2.2 Model parameters

To perform the segmentation, the SamGeo instance was generated, since it segments the entire image and stores the output as a mask file. Each mask delineates the foreground of the image, and each mask has a distinct value. The result is a non-classified segmented image that was converted to vector shapes. To use automatic mask generator, these parameters were tuned (Table 3). The automatic mask generator creates a specific number of points in the image based on the parameter points_per_side, which controls the density of point sampling. More points can result in more detailed segmentation but may increase computational load. The Intersection over Union (IoU) parameter helps ensure segmentation quality by eliminating masks with low IoU scores. The stability score threshold ensures the segmentation results are consistent and not overly sensitive to minor changes in the model's output. Box Non-Maximal Suppression Threshold is responsible for removing overlapping bounding boxes and determines how much overlap is permissible. These parameters set the thresholds for removing low-quality or duplicate masks.

Table 3. Fine tuned parameters of the SAM automatic mask generator

Parameters	Definition	Range of test values
points_per_side	This parameter specifies the number of points to sample along one side of an image. The total number of points sampled for segmentation will be **points_per_side ** 2**.	32 (default) - 200 points
pred_iou_thresh (Prediction IOU Threshold)	This is a threshold value used to filter out segmentations based on their predicted Intersection Over Union (IOU) score. Only segmentations with an IOU score above this threshold are considered.	0.60-0.88
stability_score_thresh	This threshold is used to filter segmentations based on the stability of their mask predictions under changes to the cutoff used for binarization.	0.60-0.95
box_nms_thresh (Box Non-Maximal Suppression	This is the IOU threshold used in Non-Maximal Suppression for filtering duplicate masks. NMS is a technique to remove	0.2-0.8

Threshold)	overlapping bounding boxes, and this threshold helps in determining how much overlap is permissible. Ranges from 0-1	

4.2.3. Zero shot segmentation and post-processing

The initial runs of SAM were performed on a smaller subset of the study area and inspected visually while adjusting the parameters. The June images were used for the segmentation. After the best parameters were chosen, each area/image was tiled to be processed separately, as processing the entire image is computationally demanding. The images were turned into tiles with 800 × 800 rows and columns, while keeping the same resolution. A padding of 50 pixels was also used to ensure that the areas overlap. Post-processing steps included removing elongated objects such as fallen wood from the raster masks using a measure for roundness. The roundness of each object was calculated using the formula in Equation (2)

$$Roundness = \frac{4\pi \times Area}{Perimeter^2}$$

.....(2)

which quantifies how closely the shape of the object approximates a circle. Objects with roundness values below a certain threshold were considered elongated and were filtered out from the vector results.

4.2.4 Validation data creation

Validation data were created from a randomized subset the June images and were semi-automatically digitized using the QGIS SAM plugin, an interactive tool that can be used in QGIS that implements SAMs prompting functionalities (Zhao, 2023), which allows for promptable segmentation with box boundaries. 20% of the tiles were randomly selected and digitized. Trees were digitized using semi-automatic segmentation and labelled as non-spruce and Norway spruce trees. Bounding box prompts and points were used as a prompt to the model, directly creating object masks from the input image. Then, trees that were not detected in the segmentation prompts were digitized by hand. The semi-automatic segmentation will also be discussed and presented in the results. A total of about 1500 trees were digitized using the QGIS SAM plug in. This digitization was done in a semi-automated manner, meaning that

the bounding box feature of SAM was used to identify individual trees in the images (Figure 6). Point prompts were also explored to compare the output masks of box and point prompts. A total of 358 spruce trees were digitized from the 1500 digitized trees.

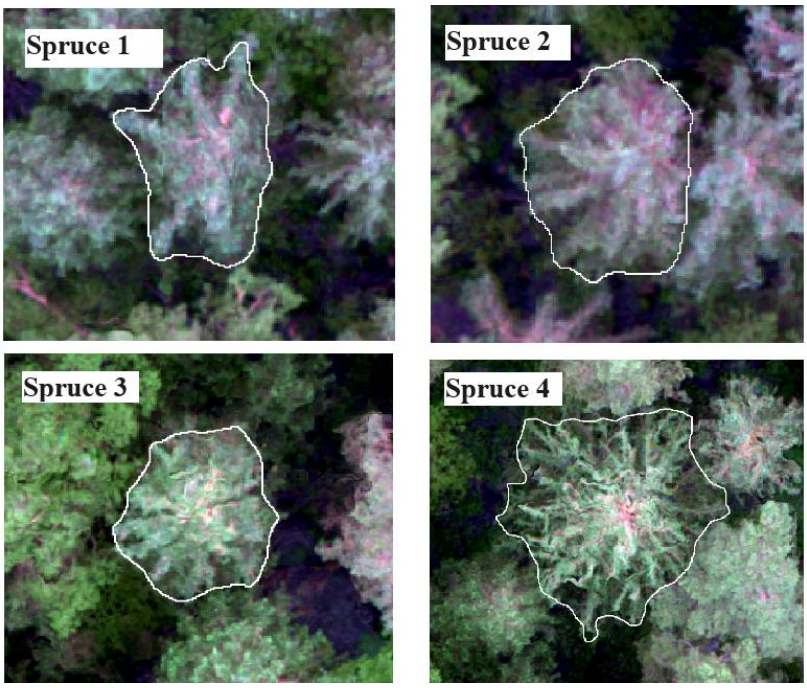

Figure 6. Examples of labelled validation data for spruce trees.

4.2.5 SAM evaluation metrics

Intersection over Union (IoU)

To validate SAM, intersection over union (IoU), tree count, canopy fractional cover, and tree area comparison will be used. The focus will be on analysing only spruce trees since this is the tree of interest. The IoU metric, a widely used method in image segmentation tasks, provides a quantitative measure of overlap between two areas - in this case, the segmented tree crowns (validation data) and those identified by SAM segmentation algorithm (Figure 7).

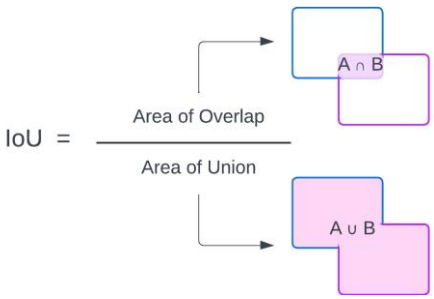

Figure 7. IoU calculation for the vectors mask output of SAM and validation masks.

For each tree crown,the area where the model's segmentation overlaps with the manual segmentation (Intersection) was calculated. Then the combined area of both segmentations (Union) was calculated. The IoU score is the ratio of these two areas, providing a value between 0 and 1. An IoU of 1 indicates perfect overlap, whereas an IoU of 0 signifies no overlap. Higher IoU scores thus reflect greater accuracy of the model in replicating manual segmentation.

Tree count and canopy fractional cover

Tree count is another metric to validate the outputs, where the validation data is compared to the generated masks produced by SAM. Moreover, grid cells were created per image to count the trees in each grid to qualitatively compare the SAM output to the validation data. The tree count then is counted per tree centroid within each grid cell, resulting in a tree count. Similarly, canopy fractional cover is calculated as the ratio of the vegetated area and non-vegetated area (Figure 8). This is calculated per grid cell in the validation data and compared to the mask vector data as shown in Equation (3) It ranges from 0 to 1, which are normalized values from the global maximum and minimum of canopy fractional covers derived from the validation data. The number on the grid cells represent the tree counts.

$$Fractional\ Canopy\ Cover\ = \frac{Area\ of\ tree\ polygon\ in\ grid\ cell}{Total\ area\ of\ grid\ cell} \quad \text{..... (3)}$$

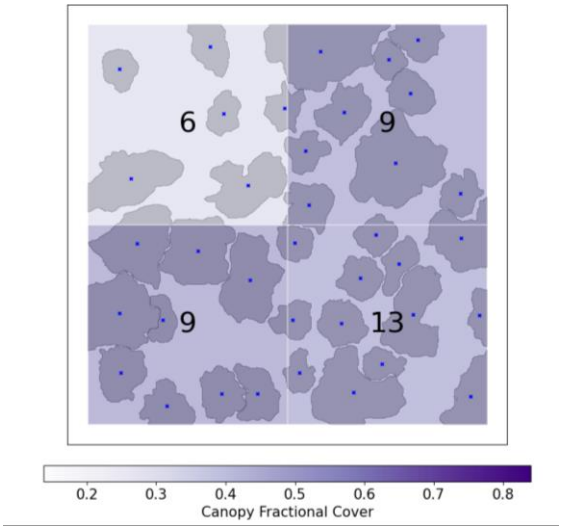

Figure 8. Calculation of canopy fractional cover and tree count per grid cell. The blue point are the tree centroids and the number on the cells represent the tree counts per cell, while the shading is indicative of the canopy fractional cover.

4.3 Vegetation Indices calculation and time series

Creation of tree segments

Points collected during the field collection were used as a reference to digitize the infected trees. To find the location of the trees, RGB orthomosaics for June, August, October, and November images were compared to find declining spruce trees in proximity to the points collected in the field. Since the accuracy of the GPS is low in the forest, and some trees were on the edge of the orthomosaics, a few trees were omitted resulting in 4 infected trees in total. Healthy trees were randomized as close by trees as a reference for the time series calculations. These were used as the regions to calculate each mean vegetation index values.

Index calculations

The standard RGB bands were used to calculate chromatic coordinates, which have the capability to monitor the phenology of trees in a forest. The Green Chromatic Coordinate (GCC; Eq. 4) and Red Chromatic Coordinate (RCC; Eq. 5) are an example of such coordinates that can be retrieved from RGB bands.

$$GCC = \frac{DN_G}{(DN_R + DN_G + DN_B)}$$

.....(4)

$$RCC = \frac{DN_R}{(DN_R + DN_G + DN_B)}$$

.....(5)

Where DNR, DNG, and DN_B are the mean digital numbers for the R, G,and B channels. The Mean RCC and GCC are computed from the tree segmented areas, for both healthy and attacked trees. Moreover, vegetation indices such as Normalized Difference Vegetation Index (NDVI; Eq. 6) and Normalized Difference Red-Edge Index (NDRE; Eq. 7) were also calculated. NDVI was calculated using the uncalibrated NIR and R band, while NDRE was calculated using the radiometrically calibrated NIR and Red-Edge bands.

$$NDVI = \frac{DN_{NIR} - DN_R}{DNI_R + DN_{NIR}}$$

.....(6)

$$NDRE = \frac{NIR - RedEdge}{NIR + RedEdge}$$

.....(7)

Additionally, the one standard deviation was measured for all the points in each time step.

Extraction of time series and statistical testing

The time series were extracted using digitized tree polygons from collected tree point data. Zonal statistics were used to extract mean values per tree per flight date, and these were averaged to produce the time series plots. The standard deviation for each tree was also calculated and plotted with the mean plots. To determine whether differences in indices were statistically significant, a Mann Whittney U test was performed. This is to account for the lack of normality in the data, so a non-parametric test was used with the Scipy module in python.

5 Results

As part of utilizing SAM was to create validation data, below is the results of using the box and point prompt feature of SAM. The box prompts yield better results than the point prompts, as seen from the figure below. Although the box prompt creates valid masks for validation, it still misses a few trees. The box prompts also have no issues with spruce trees, as it segments them well, except for a few cases where

several trees are merged into one bigger polygon. This issue is more apparent with the point prompts, where the trees are segmented into even larger polygons (Figure 9). However, there are certain cases that it can detect trees better than the box prompts. The semi-automated method worked for some trees, but some trees were missed by the box prompts, these had to be digitized manually. Tile 3 was completely missed by the point inputs, delineating the whole region as one object. Tile 4 and Tile 2 were segmented well with both the boxes and the points, with the boxes segmenting in better detail than the points.

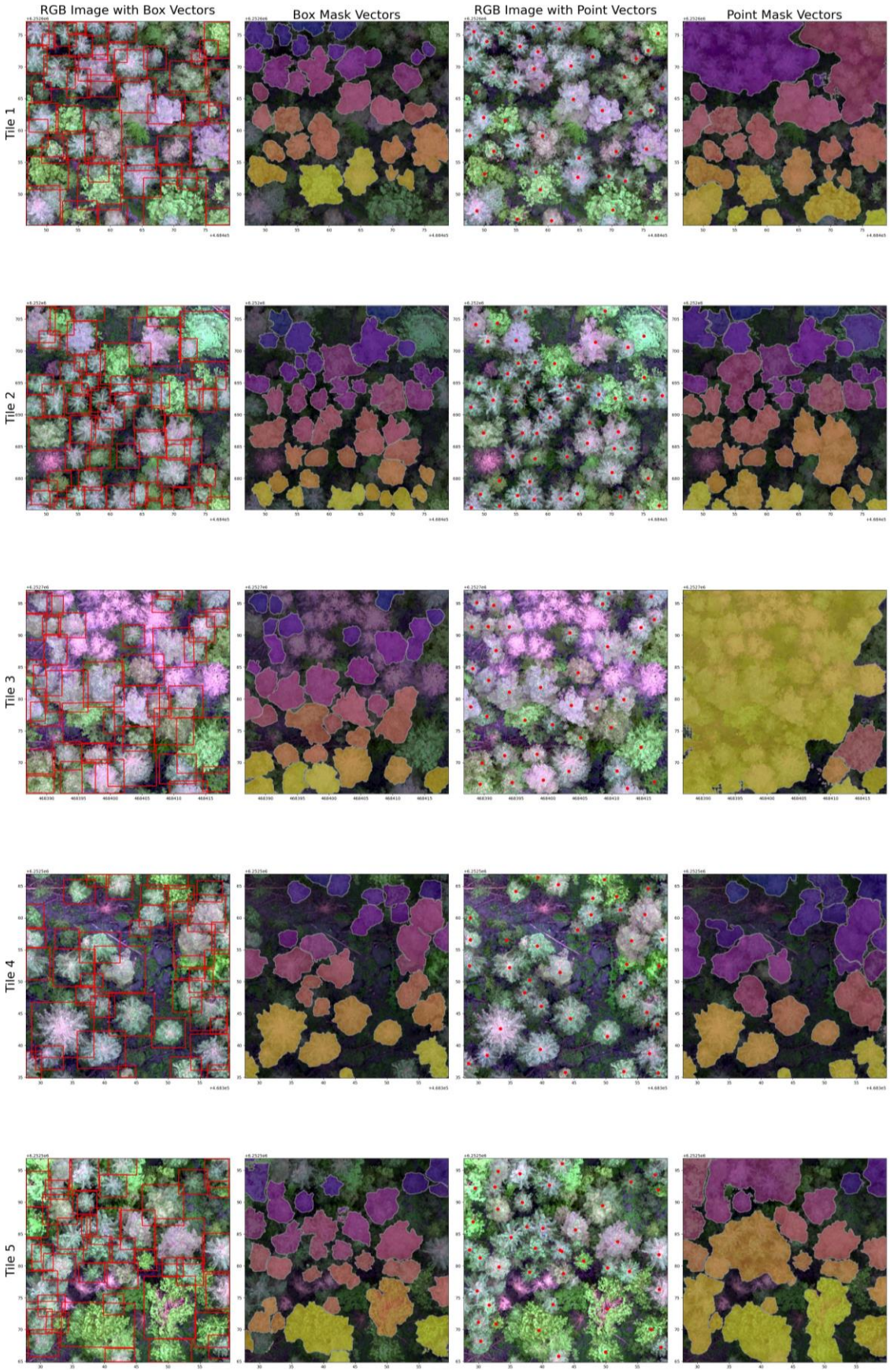

Figure 9. Box prompts and point prompts for validation data creation and their corresponding vector masks.

The parameters that were first used were the default settings. By visual comparison, we can see that the algorithm is able to detect some individual trees but oftentimes merges canopies into one object. An increase in the parameter number of points resulted in better detail, but at the expense of increased computational time (Figure 10).

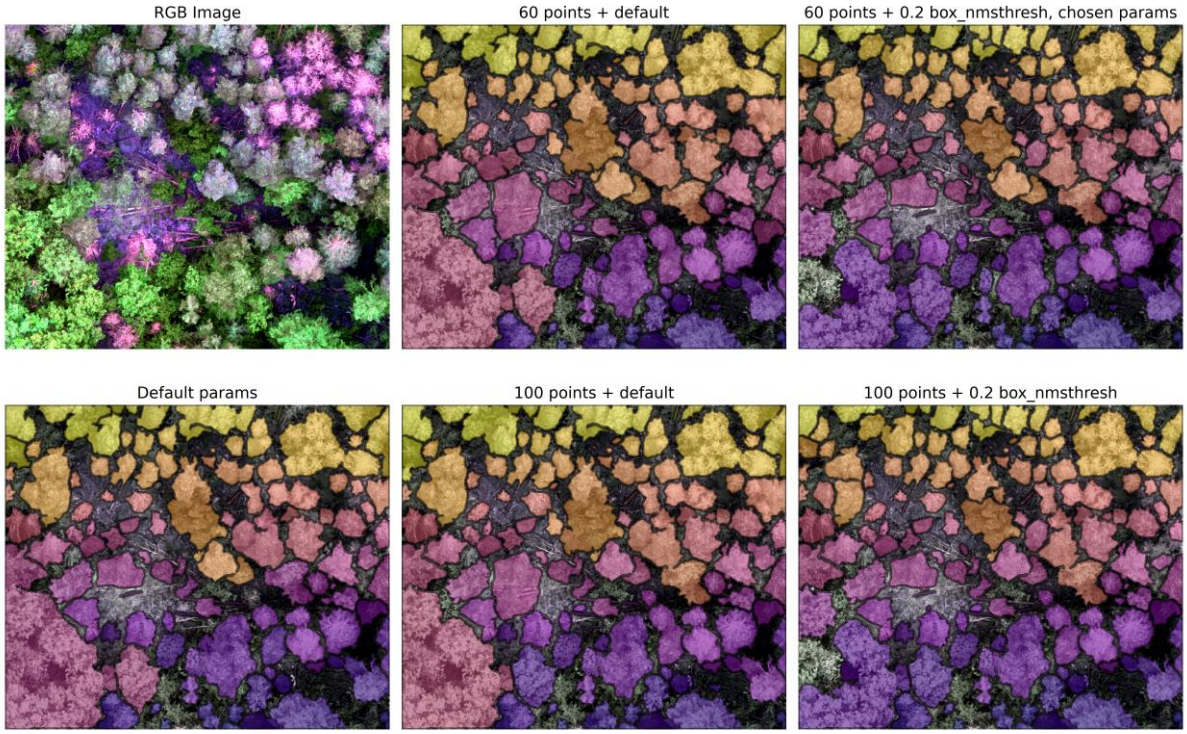

Figure 10. Fine tuning the parameters from subset image. RGB image is shown and overlaid with the different trials, default, 60 points, 100 points,m and changes in box_nms threshold.

Changing the parameter “points per side” to 60 resulted in better segmentation between individual tree crowns but has problems with ambiguous borders where canopies are merged together. The next parameter tuned was the prediction IoU threshold, which gave the best results at 0.88. Stability score threshold yielded the best results at 0.95 which distinguished trees better. Box nms at 0.2 threshold yielded the best results. Increasing the points to 100 yielded in slightly better results, but not immensely since it also merged two a few trees together. 200 points yielded no difference between 100 and 200. The final parameters kept were default parameters, while changing the points to 60 points per side and 0.2 box nms thresh, which

separated the trees best visually. Since 100 points did not necessarily make the outputs better, 60 points were kept to minimize processing time.

5.1 SAM segmentation results

Comparing the tree areas between SAM generated masks and the validation data show poor agreement (Figure 11a-b). For all the trees, the R^2 value is 0.13, a low value of fit (Figure 11a). Moreover, the spruce trees show an even lower fit, having an R^2 of 0.11 (Figure 11b). This is contrasting with the expected results, as Norway spruce trees are easier to delineate by looking at RGB images since their canopies are very distinct. Most of the trees in the validation data are small in size, and it is rarer to find larger trees in the data. Therefore, for making this plot trees larger than the maximum size of all the trees (80m^2) were excluded from the plotting since these are already considered to be errors. There is some level of agreement, where several values fall within a straight line.

Sam segmentation results

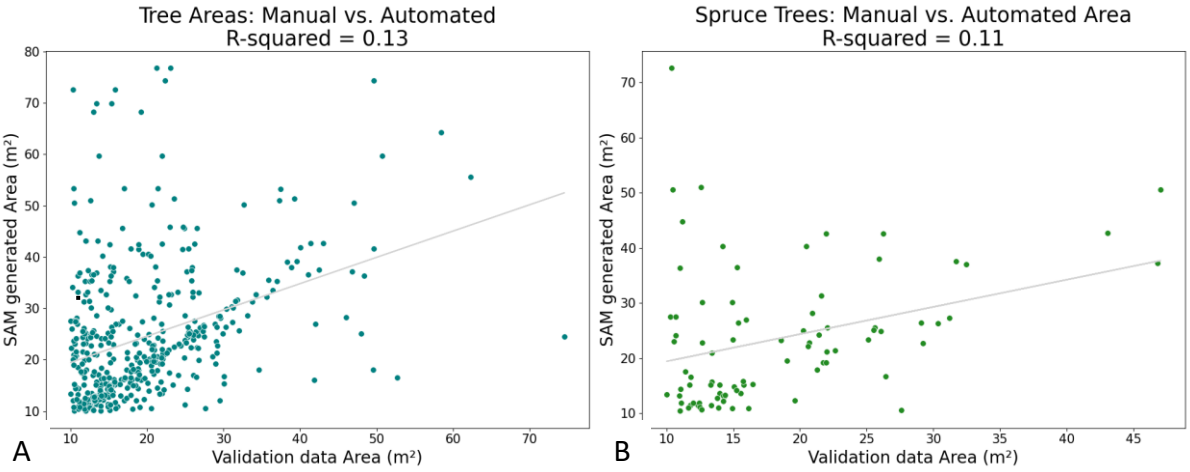

Figure 11. Plot comparison of SAM tree segments of (a) all trees and (b) Norway spruce trees and validation data.

Out of all the filtered digitized trees (1448), 549 were detected by SAM (Table 4). Among these, 307 Norway spruce trees validation data had a matching 101 trees in the SAM data. SAM was therefore able to detect 37% of all the trees, and 33% of all the spruce trees. The IoU for all trees have a value of 0.53, and 0.55 for Norway

spruce trees. This value indicates that although individual trees and their individual areas are missed by the model, the tree regions are better identified.

Table 4. Tree count of all species and Norway spruce trees generated by the SAM created masks and validation data, and IoU values for all trees and spruce trees.

Variable	**Count**
All validation trees	1448
All SAM trees	549
Spruce validation trees	307
Spruce SAM trees	101
IoU all trees	0.53
IoU spruce trees	0.55

When visually comparing the RGB images next to the masks and validation data, the canopy fractional cover and tree counts can be seen and compared to each other (Figure 10). Gemerally, SAM has a tendency to miss the detection of some trees, group them into a larger region instead of detecting individual trees and segment some non-vegetation objects as foreground (trees).

An example of the first scenario is in Figure 12a, where numerous trees are missed 6 out of 17 trees were detected. An example of the second scenario of grouping individual trees into larger regions is Figure 12b where 2 trees were detected out of 17, but this is due to the model grouping them as one larger polygon composing of several trees. Objects with similar textures and colours such as the cluster of spruce trees in Figure 12b, have a tendency to be grouped together. Figure 12d shows that SAM segments the background soil as trees at times. This, however, is not a great issue since post-processing steps can be applied to remove non-vegetation objects in the final segments. Finally, Figure 12c and 13d show SAM's strengths in segmenting, where it is capable of detecting several individual trees where the constrast between the trees and the soil is high and there is enough space between the trees to be distinguished from each other and their canopies are not overlapping. The results also show that SAM tends to miss trees in a high tree count and high canopy fractional

cover scenario (dark purple grids) (Figure 12f) and performs better when the trees are evenly spaced and less dense (Figure 12d-e).

A)

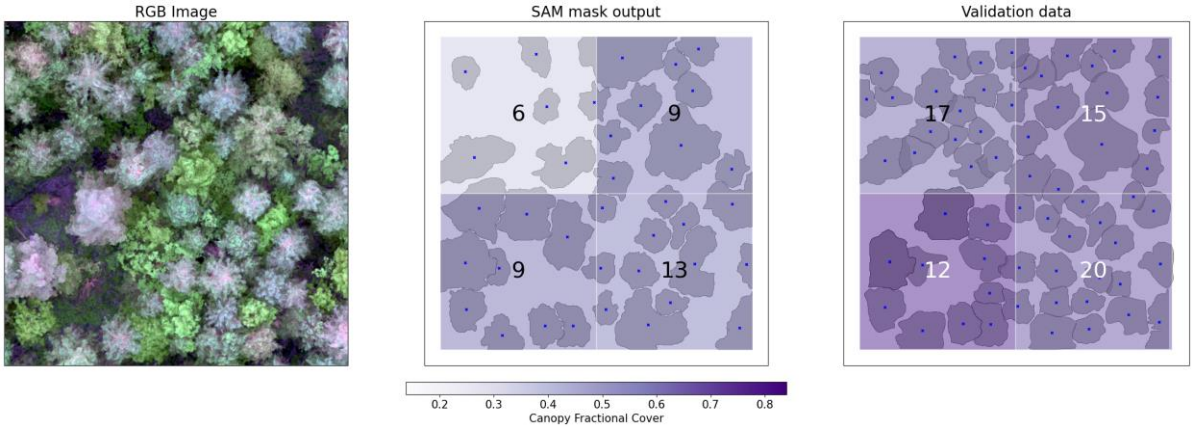

B)

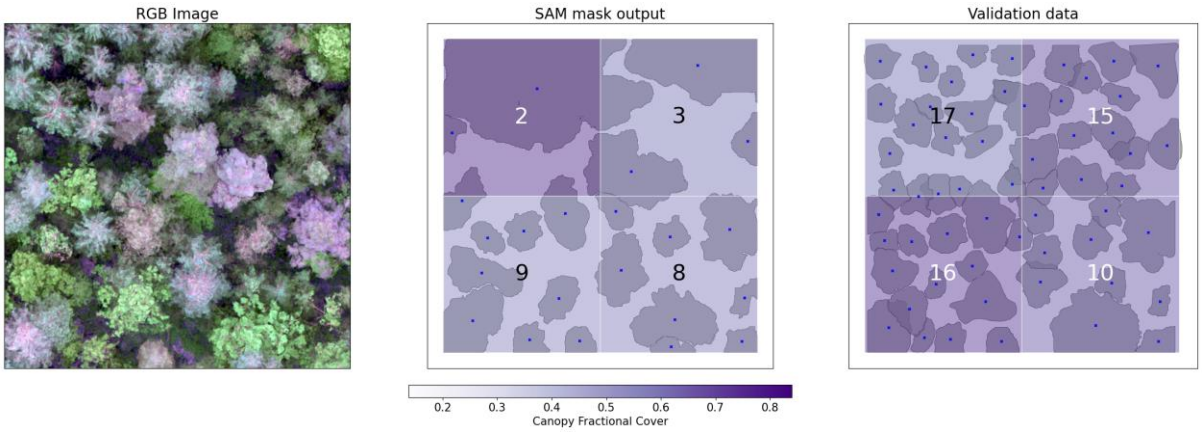

C)

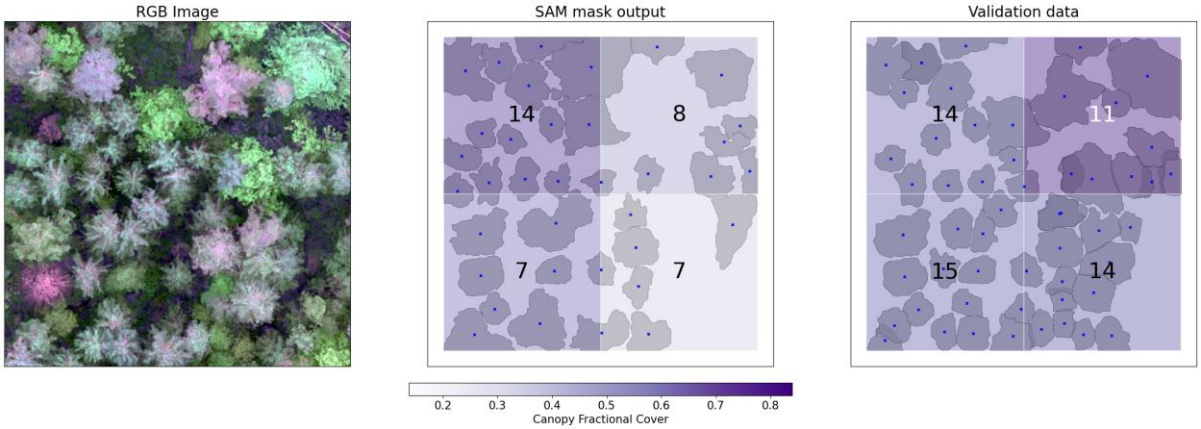
RGB Image
SAM mask output
14
8
7
7
Validation data
14
11
15
14
0.2
0.3
0.4
0.5
0.6
0.7
0.8
Canopy Fractional Cover

D)

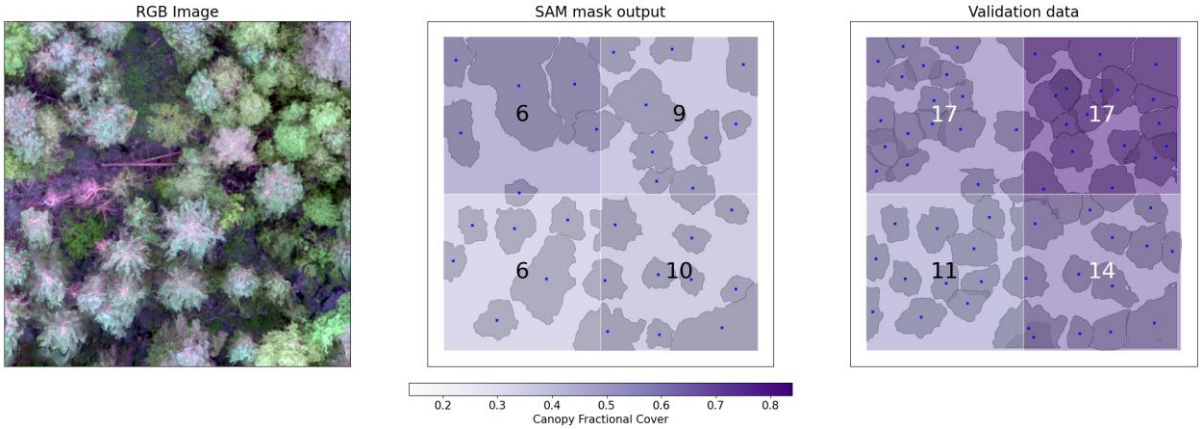
RGB Image
SAM mask output
6
9
6
10
Validation data
17
17
11
14
0.2
0.3
0.4
0.5
0.6
0.7
0.8
Canopy Fractional Cover

E)

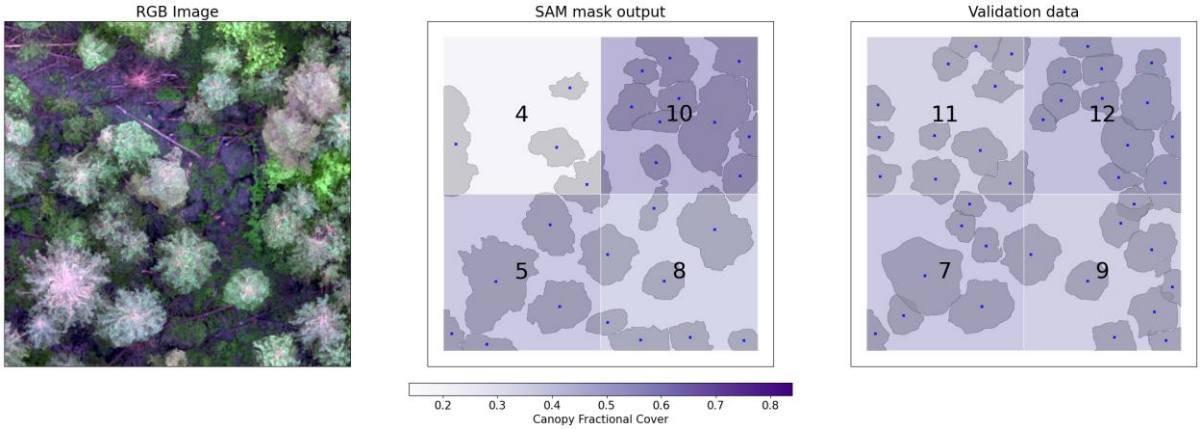
RGB Image
SAM mask output
4
10
5
8
Validation data
11
12
7
9
0.2
0.3
0.4
0.5
0.6
0.7
0.8
Canopy Fractional Cover

F)

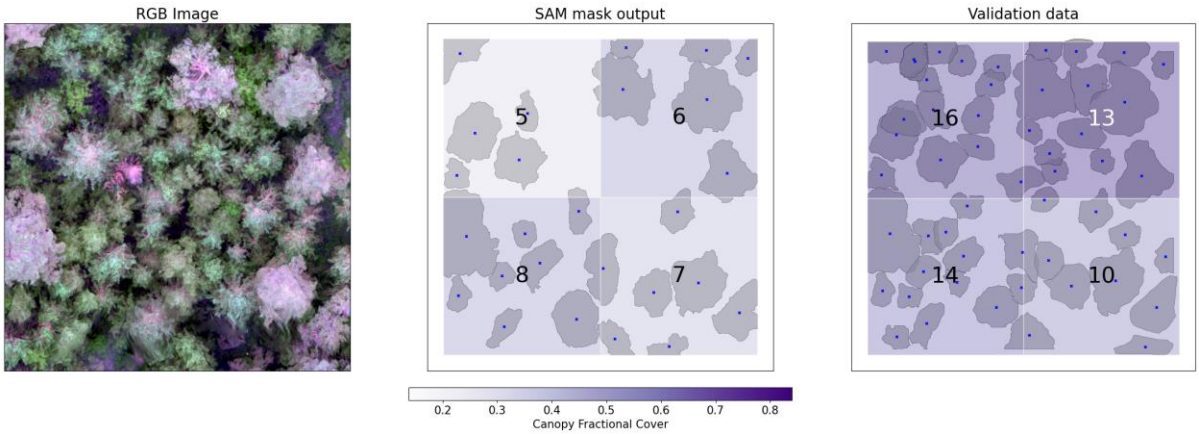

Figure 12. (A-F) Validation data subset with their corresponding canopy fractional cover and tree count and the RGB image for each. The canopy fractional cover ranges from 0 to 1 where 1 is the maximum FCC. Tree counts are displayed in the centre of each grid.

5.2 Time series of individual bands and vegetation indices

Manual segments were used to obtain tree crown areas and calculate vegetation indices. Below are time series generated from the tree segments and multispectral orthomosaics. Figures 13a-f show the calculated bands and vegetation indices per flight date. Figure a-b shows the single bands Red-Edge and NIR which were both radiometrically calibrated. Red-Edge band (Figure 13a) show that there are no notable differences between healthy and infected trees. Figure 13b shows the NIR band, showing a difference in early September. The NIR band has high variation in the data for both healthy and infected trees, but more so for the infected trees, especially towards November. Figure 13c shows NDRE, which seems to be distinguishable from late August and onwards. NDRE also decreases decreases for the infected trees over time. Figure 13d shows the GCC, which looks identifiable at an earlier date than the rest of the indices. Changes in the GCC vaues between the trees appear more pronounced than other indices. Looking at Figure 13e for RCC, a difference can also be observed from August and onwards where the values increase for the infected trees. Lastly, NDVI (Figure 13f) shows a high standard deviation, and a possible differentiation in later August.

a)

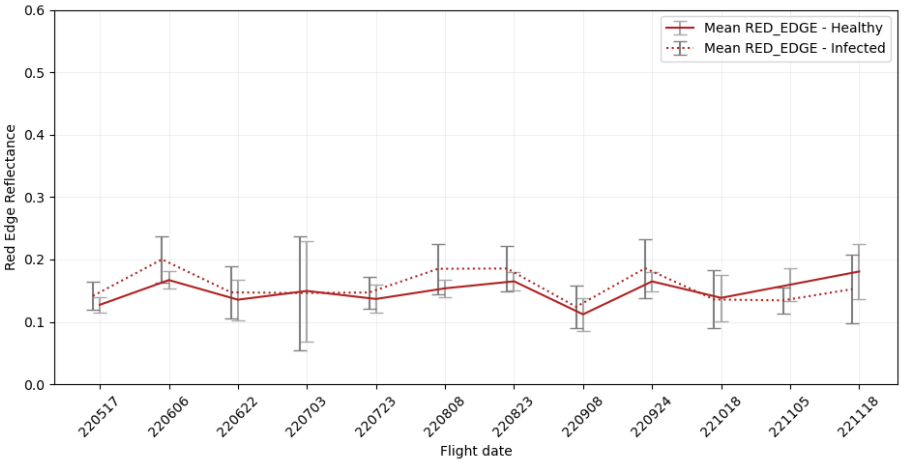
Mean RED_EDGE - Healthy
Mean RED_EDGE - Infected
Red Edge Reflectance
0.0
0.1
0.2
0.3
0.4
0.5
0.6
220517
220606
220622
220703
220723
220808
220823
220908
220924
221018
221105
221118
Flight date

b)

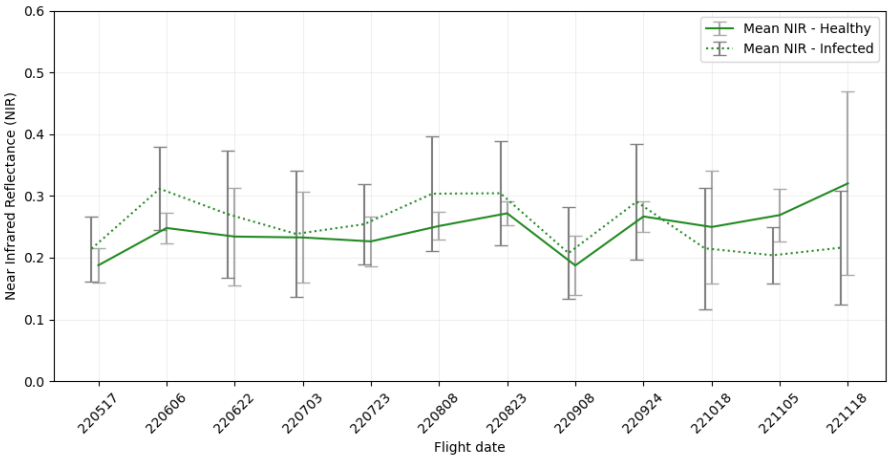
Mean NIR - Healthy
Mean NIR - Infected
Near Infrared Reflectance (NIR)
0.0
0.1
0.2
0.3
0.4
0.5
0.6
220517
220606
220622
220703
220723
220808
220823
220908
220924
221018
221105
221118
Flight date

c)

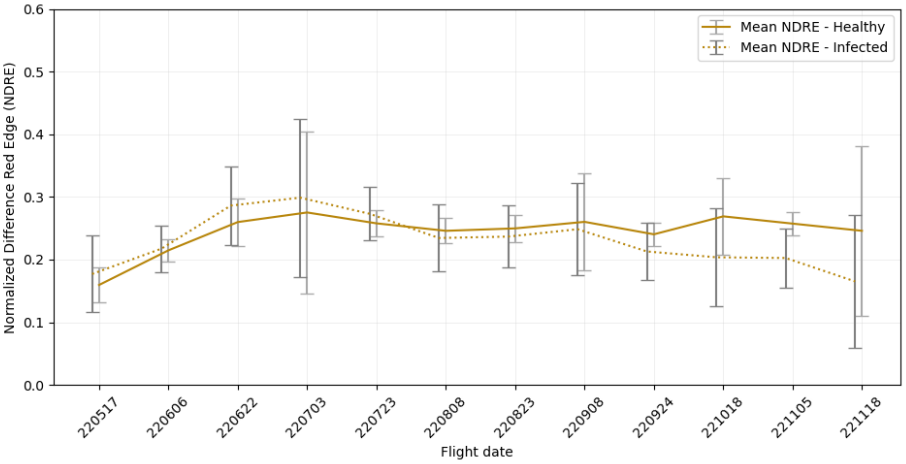
Mean NDRE - Healthy
Mean NDRE - Infected
Normalized Difference Red Edge (NDRE)
0.0
0.1
0.2
0.3
0.4
0.5
0.6
220517
220606
220622
220703
220723
220808
220823
220908
220924
221018
221105
221118
Flight date

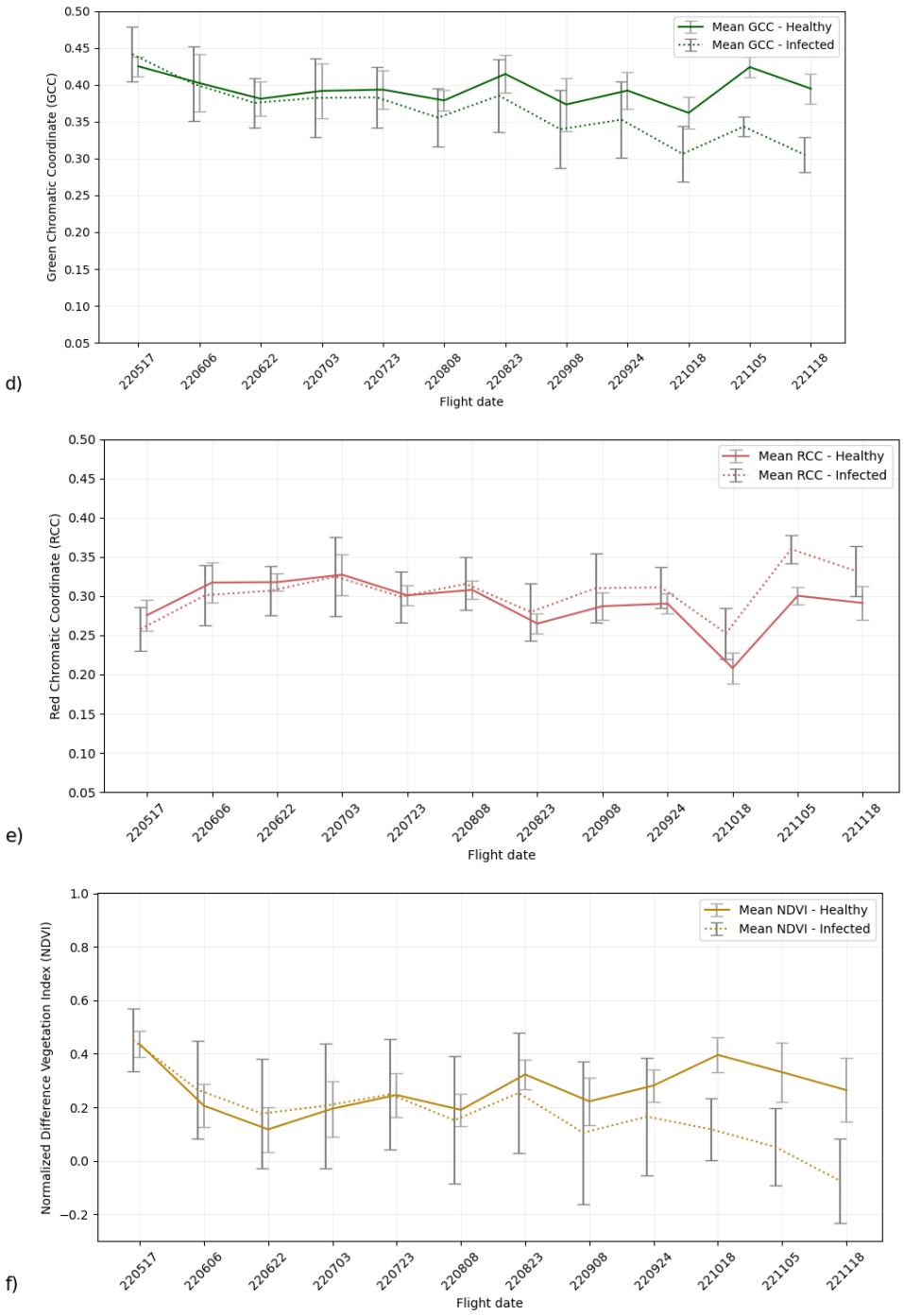

Figures 13. Vegetation Indices mean values per flight date for (a) Red-Edge band, (b) NIR band, (c) NDRE, (d) GCC, (e) RCC, and (f) NDVI bands and indices. The y-axis is the value of the indices, while the flight date is on the x-axis for all the figures.

The significance of the differences between the healthy and infected trees are illustrated in table 4. The significant values are highlighted in yellow. NDVI and GCC start to manifest significant differences between the trees in early August, and the differentiation steadily increases with time. GCC already manifests significant

differences already in early June. NDRE and NIR both show significant differences in November. Red-Edge show no significant difference at all.

Table 4. Significance < 0.05 of the vegetation indices and single bands over time

	P-value					
Date	**NDVI P**	**RCC**	**GCC**	**NDRE**	**RED_EDGE**	**NIR P**
05-17	0.1294	0.5304	0.0506	0.1483	0.3356	0.2718
06-06	0.2718	0.5749	0.0423	0.4467	0.7028	0.2431
06-22	0.0970	0.1124	0.0096	0.4467	0.0506	0.0602
07-03	0.0602	0.0602	0.1917	0.9738	0.7173	0.7173
07-23	0.1483	0.4076	0.2718	0.3048	0.3810	0.2286
08-08	0.0236	0.1690	0.0236	0.6685	0.1483	0.1294
08-23	0.0096	0.2163	0.0122	0.3027	0.2163	0.1124
09-08	0.0096	0.0122	0.0043	0.7671	0.0970	0.3027
09-24	0.0423	0.0192	3.7643E-05	0.2163	0.8694	0.8694
10-18	0.0002	0.0003	0.0002	0.6685	0.1690	0.7173
11-05	0.0005	0.0002	0.0002	0.0005	0.1734	0.0264
11-18	3.7643E-05	3.7643E-05	3.7643E-05	0.0710	0.8180	0.6210

Figure 14 shows the progression of the infected trees with time, from June – November Note that the images are not all at the same scale, so the sizes of the trees may appear different due to varying levels of zoom and do not accurately represent their true proportions. Visually, there is no noticeable difference between June and August, but the differences manifest in after October. For Tree 6, the tree has declined faster than the others, already having lost most of its needles in October.

Figure 14. Infected trees confirmed in the field and the RGB orthomosaic images and their segments. The figure shows their development over time from june to november.

6 Discussion

The discussion is divided into two parts, section 6.1 which discusses the SAM delineation of tree crowns, and section 6.2 which discuss the spectral indices and early detection.

6.1 Capability of SAM for individual tree crown delineation

This study aimed to investigate the capabilities of the Meta AI's Segment Anything Model for remote sensing applications- segmenting individual trees from high resolution UAV imagery. This section discusses the results, implications, and the limitations of using SAM for individual tree crown segmentation. The results from the box and point prompts are also discussed.

6.1.1 Point prompts and box prompts

Point prompts tend to merge multiple trees into a single object, creating broader tree regions instead of distinct individual tree crowns. This merging renders point prompts suboptimal for generating precise tree segments. The improved delineation with box prompts can be attributed to their intrinsic ability to define clear boundaries for the trees by explicitly setting the areas where the segmentation should start and end. By providing these defined bounds, box prompts ensure a more accurate and controlled segmentation process.

Although increasing the number of point prompts per object might theoretically enhance segmentation accuracy, this approach was not pursued further. Initial trials demonstrated that box prompts were not only easier to perform but also delivered satisfactory results. Fine-tuning the model by adjusting SAM parameters, such as box threshold, stability, and the number of points, significantly influenced the model output, as shown in Figure 10. The number of points improved the segmentation up to a certain threshold, beyond which no further improvement was observed. This could be due to some trees being inherently difficult for SAM to detect because of their appearance and low contrast with the background. Since point prompts have issues with delineating trees, adding more points could even result in more merged objects. This occurs because the model does not explicitly recognize each point as representing a unique object; instead, the points are candidates that might be combined into a single object, even if they correspond to several different canopies. Thus, while point prompts are automatically generated, using box prompts results in better tree delineation despite the manual effort required.

6.1.2 Automatic Mask Generation

The automatic segmentation approach, which required no prompts or training, was also analysed to assess SAM's zero-shot performance. The comparison of tree areas between SAM-generated masks and validation data showed a poor fit, with low R^2 values for all trees and Norway spruce trees. SAM tends to overestimate tree areas (Figure 11), likely due to its tendency to mask tree regions instead of individual objects.

Despite having distinct and distinguishable features, the model performed worse on spruce trees, rejecting the hypothesis that zero-shot segmentation is currently usable for the creation of vegetation indices. Furthermore, due to the merging of trees in the resulting masks, only 37% of all trees were detected and 33% of Norway Spruce trees are detected. This can be due to that in denser Norway Spruce trees areas, the trees begin to have a texture and may appear as one object since their boundaries are not clear. However, a moderate IoU indicates that SAM can segment tree regions, with better results for Norway spruce trees. This may indicate that although Norway Spruce trees are harder to delineate, their regions are slightly easier to be identified than other trees. The overall performance of the automatic mask generation is poor. This performance could be due to the feature of the point prompts in section 6.1.1: each point does not explicitly belong to a unique object; instead, the points can indeed merge several features into one. This merging of multiple point features into a single object contributes to the overestimation of tree areas and the difficulty in accurately segmenting individual tree crowns.

Figures 12a-f show a comparison between the validation data and SAM-generated masks, highlighting the strengths and weaknesses of the model. In well-spaced and high background contrast scenarios, SAM can segment a tree well. However, in areas with high canopy fractional cover and tree count, SAM fails to capture the individual crowns. Additionally, it sometimes fails to distinguish the correct foreground and background and may miss detecting tree objects altogether. This further highlight that there is room for improvements.

Thus, while automatic mask generation demonstrates some capability in segmenting tree regions, the integration of semi-automatic box prompts significantly enhances the precision of tree delineation. This combined approach can achieve satisfactory results for individual tree segmentation, highlighting the need for further refinement in zero-shot segmentation models for more complex tasks in remote sensing applications.

6.1.3. Limitations and related studies

Various studies have explored the limitations of SAM within the domain of remote sensing. SAM faces several challenges, including difficulties in segmenting objects

with complex shapes or variable appearances. In natural settings like forests, object boundaries often become indistinguishable. At its current state with zero-shot segmentation, SAM struggles to handle complex images such as those of forests.

One significant issue is SAM's tendency to select shadows or background elements during segmentation, leading to difficulties in distinguishing between background and foreground, resulting in lower performance for tasks such as tree detection in its zero-shot form (Osco et al., 2023). This problem can be mitigated by thresholding using NIR bands, as demonstrated by Huo et al. (2021), to remove shadows and background from tree segments. Additionally, SAM is primarily trained on RGB images, which prevents the utilization of additional information from multispectral data. For vegetation analysis, multispectral bands provide added value, as the spectral signature of vegetation is more apparent in the NIR band.

Despite these limitations, SAM has shown promise in various studies. Sun et al. (2024) conducted a study on crop mapping with SAM using prompts for segmentation. They concluded that segmentation remains challenging unless the parcels are large, regular in shape, and have distinct color differences from the surroundings. SAM has demonstrated successful applications in fields such as medical imaging and autonomous driving. For instance, a study on medical imaging by Stein et al. (2023) demonstrated that fine-tuning SAM with bounding boxes positively impacted the results, whereas fine-tuning without bounding boxes led to poorer outcomes.

Osco et al. (2023) further concluded that although SAM has promising capabilities, there is still significant room for improvement to address its limitations and enhance its performance for task-specific applications. Incorporating a fine-tuning step, such as transitioning from zero-shot to one-shot, shows potential for improved results with SAM. Currently, the automatic mask generator only supports points and not bounding boxes. The implications of this will be discussed in 6.1.3.

6.1.4. Prospects of SAM for tree crown delineation

SAM offers several advantages that make it a compelling choice for remote sensing applications. Its foremost feature is the ability to perform zero-shot segmentation on unseen objects and images without prior training (Kirillov et al. 2023). Another

standout feature is SAM's interactive input process, which significantly reduces the time and labour required for manual image segmentation. As AI techniques evolve, foundational models like SAM provide opportunities for further refinement tailored to specific domains. Open-source and user-friendly methods such as SAM unlock numerous possibilities for automating tedious and labour-intensive tasks. Additionally, SAM's decoupled architecture—comprising a one-time image encoder and a lightweight mask decoder—ensures computational efficiency, crucial for large-scale remote sensing applications.

However, this study demonstrated that for the detailed task of individual tree delineation, automatic mask generation without guided box prompts is insufficient. Particularly, bounding box prompts show the potential to improve the segmentation by fine tuning the model, as demonstrated by this study and supported by other studies (Stein et al. 2023; Osco et al. 2023). Combining automatic mask generation with semi-automatic box prompts and manual methods can achieve satisfactory results for individual tree segmentation. Another approach that could be useful for the future is to further automate the bounding box features, to integrate a method to automatically delineate bounding boxes from tree images and using this as prompts for the model. This could, however, introduce an uncertainty if the algorithm used is flawed and inaccurate. Performing one-shot training (where the model is trained with minimal training data) as performed by Osco et al (2023) using personalised SAM or PerSAM and PerSAM-F may also be an approach to refine SAM’s capabilities (Zhang et al. 2023). This was not investigated in this study and future studies can include an exploration on these features of SAM.

6.2 Spectral response and early detection

This study investigated the early detection of spruce bark beetle attacks using multitemporal and multispectral high-resolution images. The analysis reveals that the Green Chromatic Coordinate (GCC) can distinguish between healthy and attacked trees as early as June. The Normalized Difference Vegetation Index (NDVI) follows in early August, and the Red Chromatic Coordinate (RCC) in September. NDRE and NIR show significant differences later in the year, indicating their inefficiency for early detection. The Red-Edge band does not show significant differences between

healthy and infected trees. GCC stands out by distinguishing tree types within three weeks, with a near-significant p-value of 0.0506 in May. However, this early difference is not statistically conclusive and is therefore disregarded.

For practical mitigation, the detection time for bark beetle attacks in Sweden is about 6-9 weeks post-attack (Huo et al. 2023). Using this timeframe, only GCC is effective for early intervention. Huo et al. (2023) conducted a similar study on Norway spruce in Sweden, finding the Red-Edge band significant three weeks post-attack, and the green band five weeks post-attack, though not sufficiently to discriminate between healthy and infested trees. Their findings align with this study's results for the NIR band, which shows significant differences at 25 weeks post-attack. The discrepancy with the Red-Edge band results from Huo et al. (2023) results contrast with the findings and hypothesis of research, as the Red-Edge band is usually performing well for early attack detection. Kloucek et al (2024) show that healthy and infested trees could be distinguished at the early stage of infestation using NIR, which is contrary to the results achieved by this study.

Based on the results, flying the drone in June may provide early indications of bark beetle. However, more field-confirmed tree samples are needed for thorough testing. Various studies show the green band is vital for early detection of bark beetle infestations. For instance, Kloucek et al. (2019) in the Czech Republic found that the greenness index performed best, while NIR performed lower. Minarik et al. (2016) discovered that infested trees had higher DN values in visible wavelengths and significantly lower in NIR. These findings underscore the importance of the green and red bands for early detection, highlighting the need for further research and field validation.

Overall, the indices calculated from RGB bands, such as GCC and RCC, were sufficient to distinguish healthy trees from infected ones. Even with uncalibrated RGB bands, GCC and RCC still reflected statistically significant differences between healthy and infested trees. This indicates that high-resolution UAV RGB and multispectral images are valuable tools for forest health monitoring. In contrast, multispectral bands like NIR and Red-Edge showed little to no differentiation

between healthy and infested trees. NDVI, however, displayed differences starting in early August, with these differences increasing over time.

6.2.1. Limitations and related studies

The study's findings are limited by insufficient samples, necessitating the collection of more field data to confirm the presence of suspicious trees. The challenges of collecting field data in the forest remain, and this is not something that can necessarily change anytime soon. The data collected from the images could not be utilized due to the lack of field verification of bark beetle attacks, resulting in a lower number of trees that could be investigated. Among the 12 confirmed trees in the field, the challenge remained to find them in the images, and some points were at the edge of the study area resulting in possible distortion of the pixel values for time series calculations, so these were disregarded.

Additionally, differences in spectral signatures before the attack were not considered. This is highlighted in the study by Huo et al. (2021), which covered the period before the attacks in April, the early stage from May to July, and the middle to late stage from August to October. Their results indicated that spectral differences already existed at the beginning of the vegetation season before the attacks, suggesting that the trees were stressed prior to the beetle infestations. To account for this, flights can be performed earlier on in the year before the flight/activities of the spruce bark beetles. This is however not apparent in the data as there were no significant differences before the attack began.

6.1.3 Future studies: bark beetle health monitoring and individual tree crown delineation

The study aimed to integrate two methods to facilitate early detection of bark beetle attacks in Sweden. If the crown delineation had been successful, combining these methods could have automated the process, potentially enabling the identification of infected trees in UAV images, which could then be confirmed in the field. Future research should consider training SAM to improve its suitability for tree delineation in remote sensing applications. The vegetation index GCC shows differences as early as

three weeks after potential attacks. However, the analysis does not account for pre-attack spectral differences in the trees, which would have been interesting to investigate.

7. Conclusion

This study explores the capabilities and limitations of SAM for segmentation tasks in forest environments and investigates the early detection of spruce bark beetle attacks using multitemporal and multispectral high-resolution imagery.

First, the assessment of SAM's performance revealed that its zero-shot capabilities are inadequate for tree segmentation. SAM struggles in complex scenarios, often overestimating object boundaries and producing suboptimal segmentation outputs. Performance variability with spatial resolution further limits its effectiveness in remote sensing applications. Addressing these limitations is crucial for enhancing SAM’s applicability, particularly in forest environments. Despite these challenges, SAM's box prompts showed potential, suggesting that while its fully automated capabilities are limited, further refinement and training could improve its performance by including box prompts.

Second, the study on bark beetle attack detection found that the Green Chromatic Coordinate (GCC) is the most effective vegetation index for distinguishing attacked trees as early as June. NDVI becomes effective in August, and RCC in September, while NDRE and NIR show differences in later stages. The Red-Edge band showed no significant differences. The GCC can detect attacks within 6-9 weeks, critical for timely mitigation. Additional field-confirmed samples are needed to validate these findings.

The study highlights the need for more comprehensive data collection and the integration of early detection methods with advanced segmentation models. Future research should focus on training SAM for better tree delineation in remote sensing applications and enhancing early detection frameworks using UAV imagery. Overall, this study provides insights into Segment Anything Model’s capacity to segment with no prior training, and the early detection of bark beetle infestations and emphasizing the importance of early intervention, continuous monitoring, and model improvement for effective forest health management.

References

Alvarez-Vanhard, E., Corpetti, T., & Houet, T. (2021). UAV & satellite synergies for optical remote sensing applications: A literature review. Science of Remote Sensing, 3, 100019. https://doi.org/https://doi.org/10.1016/j.srs.2021.100019

Arnberg, W., Wastenson, L., & Lekander, B. (1973). Use of Aerial Photographs for Early Detection of Bark Beetle Infestations of Spruce. Ambio, 2(3), 77–83. http://www.jstor.org/stable/25066566

Bal, A., & Palus, H. (2023). Image Vignetting Correction Using a Deformable Radial Polynomial Model. Sensors, 23(3), 1157. https://www.mdpi.com/1424-8220/23/3/1157

Bárta, V., Lukeš, P., & Homolova, L. (2021). Early detection of bark beetle infestation in Norway spruce forests of Central Europe using Sentinel-2. International Journal of Applied Earth Observation and Geoinformation, 100. https://doi.org/10.1016/j.jag.2021.102335

Baugh, W., & Groeneveld, D. (2008). Empirical proof of the empirical line. International Journal of Remote Sensing - INT J REMOTE SENS, 29, 665-672. https://doi.org/10.1080/01431160701352162

Bentz, B. J., & Jönsson, A. M. (2015). Chapter 13 - Modeling Bark Beetle Responses to Climate Change. In F. E. Vega & R. W. Hofstetter (Eds.), Bark Beetles (pp. 533-553). Academic Press. https://doi.org/https://doi.org/10.1016/B978-0-12-417156-5.00013-7

Blackburn, G. A. (1998). Spectral indices for estimating photosynthetic pigment concentrations: A test using senescent tree leaves. International Journal of Remote Sensing, 19(4), 657-675. https://doi.org/10.1080/014311698215919

Blackburn, G. A. (2006). Hyperspectral remote sensing of plant pigments. Journal of Experimental Botany, 58(4), 855-867. https://doi.org/10.1093/jxb/erl123

CABI International. (2022). Ips typographus (eight-toothed bark beetle). In CABI Compendium. doi:10.1079/cabicompendium.28843

Carraro, A., Sozzi, M., & Marinello, F. (2023). The Segment Anything Model (SAM) for accelerating the smart farming revolution. Smart Agricultural Technology, 6, 100367. https://doi.org/https://doi.org/10.1016/j.atech.2023.100367

Carter, G. A., & Knapp, A. K. (2001). Leaf optical properties in higher plants: linking spectral characteristics to stress and chlorophyll concentration. American Journal of Botany, 88(4), 677-684. https://doi.org/https://doi.org/10.2307/2657068

Chadwick, A. J., Goodbody, T. R. H., Coops, N. C., Hervieux, A., Bater, C. W., Martens, L. A., White, B., & Röeser, D. (2020). Automatic Delineation and Height Measurement of Regenerating Conifer Crowns under Leaf-

Off Conditions Using UAV Imagery. Remote Sensing, 12(24), 4104. https://www.mdpi.com/2072-4292/12/24/4104

Delegido, J., Verrelst, J., Meza, C. M., Rivera, J. P., Alonso, L., & Moreno, J. (2013). A Red-Edge spectral index for remote sensing estimation of green LAI over agroecosystems. European Journal of Agronomy, 46, 42-52. https://doi.org/https://doi.org/10.1016/j.eja.2012.12.001

DOI 10.1088/1755-1315/17/1/012152

Fernandez-Carrillo, A., Patočka, Z., Dobrovolný, L., Franco-Nieto, A., & Revilla-Romero, B. (2020). Monitoring Bark Beetle Forest Damage in Central Europe. A Remote Sensing Approach Validated with Field Data. Remote Sensing, 12(21), 3634. https://www.mdpi.com/2072-4292/12/21/3634

FieldSITES. (2023). Scripts. GitHub. Retrieved March 28, 2024, from https://github.com/fieldSITES/scripts

Gui, B., Bhardwaj, A., & Sam, L. (2024). Evaluating the Efficacy of Segment Anything Model for Delineating Agriculture and Urban Green Spaces in Multiresolution Aerial and Spaceborne Remote Sensing Images. Remote Sensing, 16(2), 414. https://www.mdpi.com/2072-4292/16/2/414

Guo, Y., Nie, G., Gao, W., & Liao, M. (2023). 2D Semantic Segmentation: Recent Developments and Future Directions. Future Internet, 15(6).

Hlásny, T., König, L., Krokene, P., Lindner, M., Montagné-Huck, C., Müller, J., Qin, H., Raffa, K., Schelhaas, M.-J., Svoboda, M., Viiri, H., & Seidl, R. (2021). Bark Beetle Outbreaks in Europe: State of Knowledge and Ways Forward for Management. Current Forestry Reports, 7, 1-28. https://doi.org/10.1007/s40725-021-00142-x

Honkavaara, E., Näsi, R., Oliveira, R., Viljanen, N., Suomalainen, J., Khoramshahi, E., Hakala, T., Nevalainen, O., Markelin, L., Vuorinen, M., Kankaanhuhta, V., Lyytikäinen-Saarenmaa, P., & Haataja, L. (2020). USING MULTITEMPORAL HYPER- AND MULTISPECTRAL UAV IMAGING FOR DETECTING BARK BEETLE INFESTATION ON NORWAY SPRUCE. Int. Arch. Photogramm. Remote Sens. Spatial Inf. Sci., XLIII-B3-2020, 429-434. https://doi.org/10.5194/isprs-archives-XLIII-B3-2020-429-2020

Hossain, M., & Chen, D. (2019). "Segmentation for object-based image analysis (OBIA): A review of algorithms and challenges from remote sensing perspective.. ISPRS Journal of Photogrammetry and Remote Sensing, 150, 115-134. https://doi.org/10.1016/j.isprsjprs.2019.02.009

https://www.asprs.org/wp-content/uploads/pers/1959journal/sep/1959_sep_595-606.pdf

Hu, X., Xu, X., & Shi, Y. (2023). How to Efficiently Adapt Large Segmentation Model (SAM) to Medical Images. ArXiv, abs/2306.13731.

Huang, C.-y., Anderegg, W. R. L., & Asner, G. P. (2019). Remote sensing of forest die-off in the Anthropocene: From plant ecophysiology to canopy

structure. Remote Sensing of Environment, 231, 111233. https://doi.org/https://doi.org/10.1016/j.rse.2019.111233

Huo, L., Lindberg, E., Bohlin, J., & Persson, H. J. (2023). Assessing the detectability of European spruce bark beetle green attack in multispectral drone images with high spatial- and temporal resolutions. Remote Sensing of Environment, 287, 113484. https://doi.org/https://doi.org/10.1016/j.rse.2023.113484

Jactel, H., Petit, J., Desprez-Loustau, M.-L., Delzon, S., Piou, D., Battisti, A., & Koricheva, J. (2012). Drought effects on damage by forest insects and pathogens: a meta-analysis. Global Change Biology, 18(1), 267-276. https://doi.org/https://doi.org/10.1111/j.1365-2486.2011.02512.x

Jing, L., Hu, B., Li, J., Noland, T., & Guo, H. (2014). Automated tree crown delineation from imagery based on morphological techniques. IOP Conference Series: Earth and Environmental Science, 17(1), 012066. https://doi.org/10.1088/1755-1315/17/1/012066

Jönsson, A. M., L. M. Schroeder, F. Lagergren, O. Anderbrant, and B. Smith. (2012). Guess the impact of Ips typographus—an ecosystem modelling approach for simulating spruce bark beetle outbreaks. Agricultural and Forest Meteorology 166:

Kärvemo, S., Huo, L., Öhrn, P., Lindberg, E., & Persson, H. J. (2023). Different triggers, different stories: Bark-beetle infestation patterns after storm and drought-induced outbreaks. Forest Ecology and Management, 545, 121255. https://doi.org/https://doi.org/10.1016/j.foreco.2023.121255

Kautz, M., Feurer, J., & Adler, P. (2024). Early detection of bark beetle (Ips typographus) infestations by remote sensing – A critical review of recent research. Forest Ecology and Management, 556, 121595. https://doi.org/https://doi.org/10.1016/j.foreco.2023.121595

Kimoto & Dutchi-Holt. (2006). Exotic forest insect guidebook (T. Kimoto & M. Duthie-Holt, Authors). Canadian Food Inspection Agency. https://publications.gc.ca/collections/Collection/A104-23-2006E.pdf

Kirillov, A., Mintun, E., Ravi, N., Mao, H., Rolland, C., Gustafson, L., Xiao, T., Whitehead, S., Berg, A. C., Lo, W.-Y., Dollár, P., & Girshick, R. B. (2023). Segment Anything. 2023 IEEE/CVF International Conference on Computer Vision (ICCV), 3992-4003.

Kotaridis, I., & Lazaridou, M. (2021). Remote sensing image segmentation advances: A meta-analysis. ISPRS Journal of Photogrammetry and Remote Sensing, 173, 309-322. https://doi.org/https://doi.org/10.1016/j.isprsjprs.2021.01.020

Jing, L., Hu, B., Li, J., Noland, T., & Guo, H. (2014). Automated tree crown delineation from imagery based on morphological techniques. IOP Conference Series: Earth and Environmental Science, 17(1), 012066. https://doi.org/10.1088/1755-1315/17/1/012066

Lange, H., Økland, B. and Krokene, P. (2006) 'Thresholds in the life cycle of the spruce bark beetle under climate change', Interj. Complex Syst, 1648.

Lausch, A., Heurich, M., D, G., Dobner, H. J., S, G.-M., & Salbach, C. (2013). Forecasting potential bark beetle outbreaks based on spruce forest vitality using hyperspectral remote-sensing techniques at different scales. Forest Ecology and Management, 308, 76-89. https://doi.org/10.1016/j.foreco.2013.07.043

Li, Y., Wang, D., Yuan, C., Li, H., & Hu, J. (2023). Enhancing Agricultural Image Segmentation with an Agricultural Segment Anything Model Adapter. Sensors, 23(18), 7884. https://www.mdpi.com/1424-8220/23/18/7884

Lou, X., Huang, Y., Fang, L., Huang, S., Gao, H., Yang, L., Weng, Y., & Hung, I. K. u. (2022). Measuring loblolly pine crowns with drone imagery through deep learning. Journal of Forestry Research, 33(1), 227-238. https://doi.org/10.1007/s11676-021-01328-6

Lv, L., Li, X., Mao, F., Zhou, L., Xuan, J., Zhao, Y., Yu, J., Song, M., Huang, L., & Du, H. (2023). A Deep Learning Network for Individual Tree Segmentation in UAV Images with a Coupled CSPNet and Attention Mechanism. Remote Sensing, 15(18).

Länsstyrelsen Blekinge. (n.d.). *Mulatorp*. Retrieved June 18, 2024, from https://www.lansstyrelsen.se/blekinge/besoksmal/naturreservat/mulatorp.html?sv.target=12.382c024b1800285d5863a87c&sv.12.382c024b1800285d5863a87c.route=/&searchString=&counties=&municipalities=&reserveTypes=&natureTypes=&accessibility=&facilities=&sort=none

Ma, Z., He, X., Sun, S., Yan, B., Kwak, H., & Gao, J. (2023). Zero-Shot Digital Rock Image Segmentation with a Fine-Tuned Segment Anything Model. ArXiv, abs/2311.10865.

Marini, L., Lindelöw, Å., Jönsson, A. M., Wulff, S., & Schroeder, L. M. (2013). Population dynamics of the spruce bark beetle: a long-term study. Oikos, 122(12), 1768-1776. https://doi.org/https://doi.org/10.1111/j.1600-0706.2013.00431.x

Mazurowski, M., Dong, H., Gu, H., Yang, J., Konz, N., & Zhang, Y. (2023). Segment anything model for medical image analysis: An experimental study. Medical Image Analysis, 89, 102918. https://doi.org/10.1016/j.media.2023.102918

Migas-Mazur, R., Kycko, M., Zwijacz-Kozica, T., & Zagajewski, B. (2021). Assessment of Sentinel-2 Images, Support Vector Machines and Change Detection Algorithms for Bark Beetle Outbreaks Mapping in the Tatra Mountains. Remote Sensing, 13(16), 3314. https://www.mdpi.com/2072-4292/13/16/3314

Minařík, R., Langhammer, J., & Lendzioch, T. (2020). Automatic Tree Crown Extraction from UAS Multispectral Imagery for the Detection of Bark Beetle Disturbance in Mixed Forests. Remote Sensing, 24, 4081. https://doi.org/10.3390/rs12244081

Miraki, M., Sohrabi, H., Fatehi, P., & Kneubuehler, M. (2021). Individual tree crown delineation from high-resolution UAV images in broadleaf forest.

Ecological Informatics, 61, 101207. https://doi.org/https://doi.org/10.1016/j.ecoinf.2020.101207

Netherer, S., Panassiti, B., Pennerstorfer, J., & Matthews, B. (2019). Acute Drought Is an Important Driver of Bark Beetle Infestation in Austrian Norway Spruce Stands [Original Research]. Frontiers in Forests and Global Change, 2. https://doi.org/10.3389/ffgc.2019.00039

Näsi, R., Honkavaara, E., Blomqvist, M., Lyytikäinen-Saarenmaa, P., Hakala, T., Viljanen, N., Kantola, T., & Holopainen, M. (2018). Remote sensing of bark beetle damage in urban forests at individual tree level using a novel hyperspectral camera from UAV and aircraft. Urban Forestry & Urban Greening, 30, 72-83. https://doi.org/https://doi.org/10.1016/j.ufug.2018.01.010

Öhrn, P. (2012). Seasonal flight patterns of the Spruce bark beetle (Ips typographus) in Sweden : phenology, voltinism and development [Licentiate thesis, Swedish University of Agricultural Sciences]. Sveriges lantbruksuniversitet https://res.slu.se/id/publ/79084

Økland, B., S. Netherer, and L. Marini. (2015). The Eurasian spruce bark beetle: The role of climate. Climate change and insect pests 202-219.

Olsson, P. O., Bergman, H., & Piltz, K. (2023). Exploring the potential to use in-between pixel variability for early detection of bark beetle attacked trees. AGILE GIScience Ser., 4, 35. https://doi.org/10.5194/agile-giss-4-35-2023

Olsson, P.-O., Vivekar, A., Adler, K., Garcia Millan, V. E., Koc, A., Alamrani, M., & Eklundh, L. (2021). Radiometric Correction of Multispectral UAS Images: Evaluating the Accuracy of the Parrot Sequoia Camera and Sunshine Sensor. Remote Sensing, 13(4), 577. https://www.mdpi.com/2072-4292/13/4/577

Ortiz, S. M., Breidenbach, J., & Kändler, G. (2013). Early Detection of Bark Beetle Green Attack Using TerraSAR-X and RapidEye Data. Remote Sensing, 5(4), 1912-1931. https://www.mdpi.com/2072-4292/5/4/1912

Osco, L. P., Wu, Q., de Lemos, E. L., Gonçalves, W. N., Ramos, A. P. M., Li, J., & Marcato, J. (2023). The Segment Anything Model (SAM) for remote sensing applications: From zero to one shot. International Journal of Applied Earth Observation and Geoinformation, 124, 103540. https://doi.org/https://doi.org/10.1016/j.jag.2023.103540

Parra, L. (2022). Remote Sensing and GIS in Environmental Monitoring. Applied Sciences, 12(16), 8045. https://www.mdpi.com/2076-3417/12/16/8045

Photogramm. Eng., 25 (1959), pp. 595-606

Qiu, L., Jing, L., Hu, B., Li, H., & Tang, Y. (2020). A New Individual Tree Crown Delineation Method for High Resolution Multispectral Imagery. Remote Sensing, 12(3).

Qiu, L., Jing, L., Hu, B., Li, H., & Tang, Y. (2020). A New Individual Tree Crown Delineation Method for High Resolution Multispectral Imagery. Remote Sensing, 12(3), 585. https://www.mdpi.com/2072-4292/12/3/585

Heller, R. C., R. C. Aldrich, and W. F. Bailey. 1959. An evaluation of aerial photography for detecting southern pine beetle (Dendroctonus frontalis) damage . Photogrammetric Engineering 25:595-606.

Richardson, A. D., Hufkens, K., Milliman, T., & Frolking, S. (2018). Intercomparison of phenological transition dates derived from the PhenoCam Dataset V1.0 and MODIS satellite remote sensing. Scientific Reports, 8(1), 5679. https://doi.org/10.1038/s41598-018-23804-6

Safonova, A., Tabik, S., Alcaraz-Segura, D., Rubtsov, A., Maglinets, Y., & Herrera, F. (2019). Detection of Fir Trees (Abies sibirica) Damaged by the Bark Beetle in Unmanned Aerial Vehicle Images with Deep Learning. Remote Sensing, 11(6), 643. https://www.mdpi.com/2072-4292/11/6/643

Schelhaas, M.-J., Nabuurs, G.-J., & Schuck, A. (2003). Natural disturbances in the European forests in the 19th and 20th centuries. Global Change Biology, 9, 1620-1633. https://doi.org/10.1046/j.1365-2486.2003.00684.x

Schroeder, M. (2023). Skyddade områden och granbarkborre - en kunskapssammanställning med fokus på biologi, spridning av angrepp och bekämpning Rapport Skog 2023:3. Sveriges lantbruksuniversitet, Umeå. 45 sidor

Seidl, R., Thom, D., Kautz, M., Martin-Benito, D., Peltoniemi, M., Vacchiano, G., Wild, J., Ascoli, D., Petr, M., Honkaniemi, J., Lexer, M. J., Trotsiuk, V., Mairota, P., Svoboda, M., Fabrika, M., Nagel, T. A., & Reyer, C. P. O. (2017). Forest disturbances under climate change. Nature Climate Change, 7(6), 395-402. https://doi.org/10.1038/nclimate3303

Smith, G. M., & Milton, E. J. (1999). The use of the empirical line method to calibrate remotely sensed data to reflectance. International Journal of Remote Sensing, 20(13), 2653-2662. https://doi.org/10.1080/014311699211994

Sommerfeld, A., Rammer, W., Heurich, M., Hilmers, T., Müller, J., & Seidl, R. (2021). Do bark beetle outbreaks amplify or dampen future bark beetle disturbances in Central Europe? Journal of Ecology, 109(2), 737-749. https://doi.org/10.1111/1365-2745.13502

Stein, J., Folco, M. D., & Schnabel, J. A. (2023). Influence of Prompting Strategies on Segment Anything Model (SAM) for Short-axis Cardiac MRI segmentation. Bildverarbeitung für die Medizin,

Sun, J., Yan, S., Alexandridis, T., Yao, X., Zhou, H., Gao, B., Huang, J., Yang, J., & Li, Y. (2024). Enhancing Crop Mapping through Automated Sample Generation Based on Segment Anything Model with Medium-Resolution Satellite Imagery. Remote Sensing, 16(9), 1505. https://www.mdpi.com/2072-4292/16/9/1505

Thapa, S., Garcia Millan, V. E., & Eklundh, L. (2021). Assessing forest phenology: A multi-scale comparison of near-surface (UAV, spectral reflectance sensor, PhenoCam) and satellite (MODIS, Sentinel-2) remote sensing. Remote Sensing, 13(8), 1597. https://www.mdpi.com/2072-4292/13/8/1597

Trubin, A., Kozhoridze, G., Zabihi, K., Modlinger, R., Singh, V. V., Surový, P., & Jakuš, R. (2023). Detection of susceptible Norway spruce to bark beetle attack using PlanetScope multispectral imagery [Original Research]. Frontiers in Forests and Global Change, 6. https://doi.org/10.3389/ffgc.2023.1130721

Turkulainen, E., Honkavaara, E., Näsi, R., Oliveira, R. A., Hakala, T., Junttila, S., Karila, K., Koivumäki, N., Pelto-Arvo, M., Tuviala, J., Östersund, M., Pölönen, I., & Lyytikäinen-Saarenmaa, P. (2023). Comparison of Deep Neural Networks in the Classification of Bark Beetle-Induced Spruce Damage Using UAS Images. Remote Sensing, 15(20).

Williams, D., Macfarlane, F., & Britten, A. (2023). Leaf Only SAM: A Segment Anything Pipeline for Zero-Shot Automated Leaf Segmentation.

Wu, J., Yang, G., Yang, H., Zhu, Y., Li, Z., Lei, L., & Zhao, C. (2020). Extracting apple tree crown information from remote imagery using deep learning. Computers and Electronics in Agriculture, 174, 105504. https://doi.org/https://doi.org/10.1016/j.compag.2020.105504

Wulder, M., White, J., Bentz, B., Alvarez-Taboada, F., & Coops, N. (2006). Estimating the probability of mountain pine beetle red-attack damage. Remote Sensing of Environment, 101, 150-166. https://doi.org/10.1016/j.rse.2005.12.010

Xiao, C., Qin, R., & Huang, X. (2020). Treetop detection using convolutional neural networks trained through automatically generated pseudo labels. International Journal of Remote Sensing, 41(8), 3010-3030. https://doi.org/10.1080/01431161.2019.1698075

Yuill J.S., Eaton C.B. (1949) The airplane in forest-pest control. In: U.S. Department of Agriculture (ed.), Yearbook of agriculture 1949, Washington, D.C., p. 471–476.

Zabihi, K., Surovy, P., Trubin, A., Singh, V. V., & Jakuš, R. (2021). A review of major factors influencing the accuracy of mapping green-attack stage of bark beetle infestations using satellite imagery: Prospects to avoid data redundancy. Remote Sensing Applications: Society and Environment, 24, 100638. https://doi.org/https://doi.org/10.1016/j.rsase.2021.100638

Zeng, Y., Hao, D., Huete, A., Dechant, B., Berry, J., Chen, J. M., Joiner, J., Frankenberg, C., Bond-Lamberty, B., Ryu, Y., Xiao, J., Asrar, G. R., & Chen, M. (2022). Optical vegetation indices for monitoring terrestrial ecosystems globally. Nature Reviews Earth & Environment, 3(7), 477-493. https://doi.org/10.1038/s43017-022-00298-5

Zhao, Zhuoyi, Fan, Chengyan, & Liu, Lin. (2023). Geo SAM: A QGIS plugin using Segment Anything Model (SAM) to accelerate geospatial image segmentation (1.1.0). Zenodo. https://doi.org/10.5281/zenodo.8191039zhao